NASA-CR-197220

NASA Contractor Report XXXX

LINEAR AND NONLINEAR DYNAMIC ANALYSIS OF REDUNDANT LOAD PATH BEARINGLESS ROTOR SYSTEMS

V.R. Murthy and Louis A. Shultz
Department of Mechanical, Aerospace and Manufacturing Engineering
Syracuse University
Syracuse, New York

Prepared for

Ames Research Center
Under Grant NAG 2-306
October 1994

NASA
National Aeronautics
and Space Administration
Scientific and Technical
Information Branch
1994

PREFACE

This research was sponsored by the NASA-Ames Research Center, California under Grant No. 2-306. Randall L. Peterson was the technical monitor of the project. Several graduate students at Syracuse University participated in the program including Louis A. Shultz, Arun M. Joshi and Daniel M. Lauzon.

SUMMARY

A direct transfer matrix method is developed to analyze the linear and nonlinear dynamics of multiple-load-path bearingless rotor blades. The method is applied to determine (1) the natural frequencies and modes about the initial state, (2) the nonlinear steady state deflections, (3) the natural frequencies and modes about the steady deformed state and (4) aeroelastic stability of multiple-load-path rotor blades in hover. A Newton-Raphson iterative method based on quasilinearization of the nonlinear distributed boundary value problem is developed to solve the steady state deflections of the blade. Aerodynamic forces are calculated employing two dimensional strip theory and quasi-steady aerodynamics. The formulation is validated by comparing the results for single and multiple-load-path blades with those obtained by other methods in the literature. For forward flight applications a discretization based on either modal coordinates or harmonic analysis is recommended.

TABLE OF CONTENTS

TABLE OF CONTENTS (cont'd)

LIST OF TABLES

LIST OF FIGURES

LIST OF FIGURES (Cont'd)

LIST OF SYMBOLS

a	lift curve slope, per rad
A	area of cross-section, in^2
b	semichord (in), also number of blades
B_1^*, B_2^*	cross-section integrals (in^6, in^5), reference [40]
c	chord (in), also particular (nonhomogeneous) solution to matrix differential equation
c_d	drag coefficient
C_T	thrust coefficient
c_l	lift coefficient
c_m	pitching moment coefficient
C_l, C_l^*	cross-section integrals (in^6,in^5), reference [40]
e	mass centroid offset from elastic axis, positive when in front of the elastic axis, in
e_A	distance between area centroid (tensile axis) and elastic axis, positive for centroid forward, in
e_c	distance between quarter-chord point and shear center positive for shear center aft, in
E	Young's modulus, lb/in^2
{f}	column vector of nonhomogeneous terms in matrix differential equation
G	shear modulus, lb/in

LIST OF SYMBOLS (cont'd)

h	plunging motion, in
I_y	cross-section moment of inertia about y-axis, in^4
I_{y_o}	reference moment of inertia for non-dimensionalization, in^4
I_z	cross-section moment of inertia about z-axis, in^4
J	St. Venants torsional stiffness constant, in^4
k_A	polar radius of gyration of cross-sectional area effective in carrying tensile stresses about elastic axis, in
k_m	mass radius of gyration of blade cross section $k_m^2 = k_{m1}^2 + k_{m2}^2$, in^2
k_{m1}, k_{m2}	cross-section integrals (in), reference [40]
l	length of the load paths (in), also lift, lb/in
L_v, L_w	aerodynamic forces, lb
m	mass per unit length ($lb\text{-}sec^2/in^2$), also section pitching moment, lb
m_o	reference mass for non-dimensionalization, $lb\text{-}sec^2/in^2$
M_e	aerodynamic pitching moment about elastic axis, $lb\text{-}in/in^2$
M_x	twisting moment about x-axis, lb-in
M_y, M_z	bending moments about y and z axes, respectively, lb-in

LIST OF SYMBOLS (cont'd)

n	number of load paths
R	radius of the rotor, in
T	tension, lb
[T]	transfer matrix of the blade
$[T^i]$	transfer matrix of the ith load path
u,v,w	elastic displacements in the x,y,z directions, respectively, in
U	airfoil velocity (perpendicular to x' axis), in/sec
U_P,U_T	components of airfoil velocity in y', z' directions, respectively, in/sec
v_i	induced velocity, in/sec
V_x	axial force, lb
V_y,V_z	shear forces in the y and z directions, respectively, lb
x,y,z	mutually perpendicular undeformed axis system with x along the undeformed blade and y towards the leading edge, reference [40]
{z}	state vector
z_a	equation of meanline of airfoil, reference [39]
Δz	incremental solution in Newton-Raphson iterations
α	angle of attack, rad
β_{pc}	precone angle, rad

LIST OF SYMBOLS (cont'd)

ε	slope of beamwise deflection out of plane of rotation
θ	pretwist angle, rad
θ_{rc}	root collective, rad
λ	complex eigenvalue (sec^{-1})
ξ	slope of deflection in the plane of rotation
ξ^*	dummy variable of integration
ρ	density, $lb\text{-}sec^2/in^4$
σ_x	local solidity
ϕ	elastic twist about the elastic axis, rad
ω	frequency of vibration, sec^{-1}
Ω	blade rotational speed, sec^{-1}

Superscripts

'	differentiation with respect to x
·	differentiation with respect to time
-	non-dimensional quantity
i	quantities corresponding to the ith load path
qs	quasi-steady

LIST OF SYMBOLS (cont'd)

Subscripts

1	quantities at the root
2	quantities at the clevis
3	quantities at the blade tip
c/2	midchord
c/4	quarterchord
e	elastic axis
o	reference quantities for nondimensionalization or steady state trim quantities

1. INTRODUCTION

A large class of systems occurring in engineering practice consist of one dimensional beam and beamlike elements. Sometimes the systems contain either a single element or a number of elements linked together end to end in the form of a chain. Well known examples are simple beams, rotor or propeller blades, continuous beams, fuselage bulkheads, and turbine generator shafts. The transfer matrix (which is one form of frequency response matrix) is ideally suited to treat such one dimensional chainlike systems governed by linear equations. Intermediate conditions and the number of degrees of freedom have no effect on the order of the transfer matrices and depends only on the order of the governing differential equations.

Holzer [1] initially applied the transfer matrix method to determine the torsional vibrations of rods and the method is generally known as Holzer's method. Myklestad [2] applied a method analogous to Holzer's method to determine the bending–torsion modes of beams and the method is usually called Myklestad's method. Thomson [3] applied the method in a matrix form to more general vibration problems. The original application of the transfer matrix method also includes the description of steady state behaviour of four terminal electrical networks, in which case the method is commonly referred to as four–pole parameters method. Molloy [4] applied four pole parameters to study acoustical,

mechanical, and electromechanical vibration problems. Pestel and Leckie [5] have listed transfer matrices for elasto–mechanical elements up to twelfth order and the textbook contains several references on transfer matrices. Rubin [6,7] has provided a general treatment for transfer matrices and their relation to other forms of frequency response matrices. Transfer matrices have been applied to a wide variety of engineering problems by a number of researchers, including Targoff [8], Lin [9], Lin and McDaniel [10], Mercer and Seavey [11] Mead [12], Mead and Sen Gupta [13], Henderson and McDaniel [14], McDaniel [15], McDaniel and Logan [16], Murthy and Nigam [17] and Murthy and McDaniel [18,19]. These applications deal with beams, beam type periodic structures, cylindrical shells and stiffened rings.

The main advantage of the transfer matrix method is the smallness of the order of the matrices involved. The order of the transfer matrix will be equal to the number of elements in the state vector. The simplicity gives rise to several numerical difficulties in using transfer matrices. These can occur first, when calculating higher natural frequencies and their associated mode shapes and second, when intermediate geometric compatibility conditions are stiff. Despite these numerical problems transfer matrices offer an efficient means to study the dynamics of one dimensional systems. Combined with leaps in computing power, transfer matrices make it possible to tackle new classes of problems such as near real–time simulation and optimization. These new problems are feasible

because one dimensional systems can be modeled with computationally efficient transfer matrices.

The transfer matrix method is very popular for the analysis of rotor blades [20-26] and the reasons are (1) most of the time, only a few number of lower natural frequencies and their associated mode shapes are of interest, (2) no intermediate stiff conditions are involved in the calculation of frequencies, (3) the order of the frequency determinant is at the most six by six and (4) the method is very appealing for programming. In fact, several rotor dynamics programs within the helicopter organizations employ transfer matrix modeling for their blades. Examples of such programs include Myklestad program of Bell Helicopter [27] , Rotorcraft Airframe Comprehensive Aeroelastic Program (RACAP) of McDonnel Douglas Helicopter Co. [28], G400 program of United Technologies [29] , C60 Program of Boeing Helicopter and KTRAN of Sikorsky Aircraft.

All the existing helicopters employ either articulated, teetering, gimbaled or hingeless blades for their rotors to relieve high blade stresses encountered at the blade root during normal operating conditions. Examples of these rotor types are shown in Figures 1.1 through 1.4. An advanced configuration known as the bearingless rotor is currently being employed in new helicopters. The bearingless design is an attempt to realize the several best features of articulated rotors (lower vibration and gust sensitivity), teetering rotors (low cost) and hingeless rotors (high control power, superior

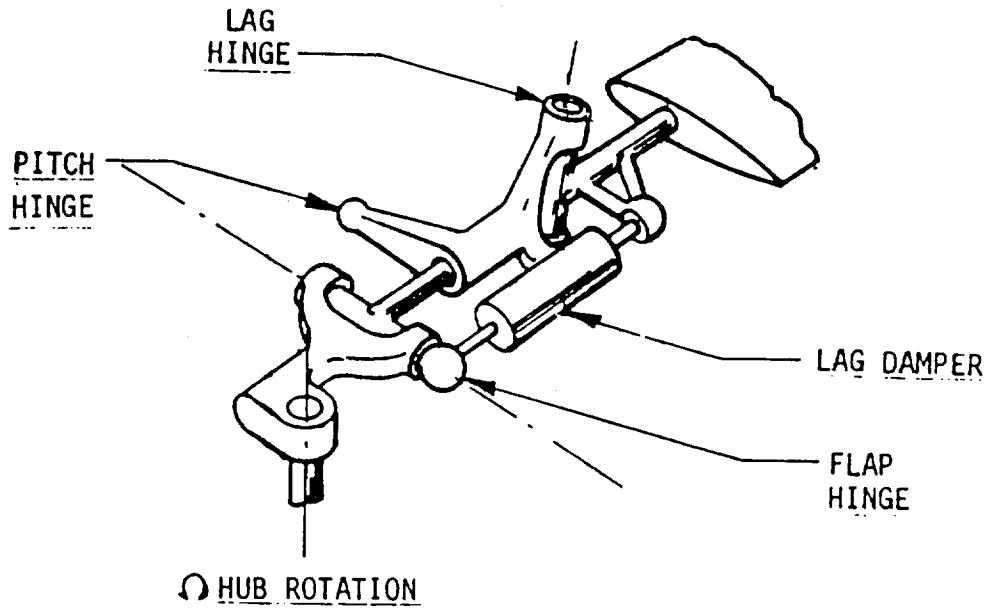

Figure 1.1 Model of An Articulated Rotor

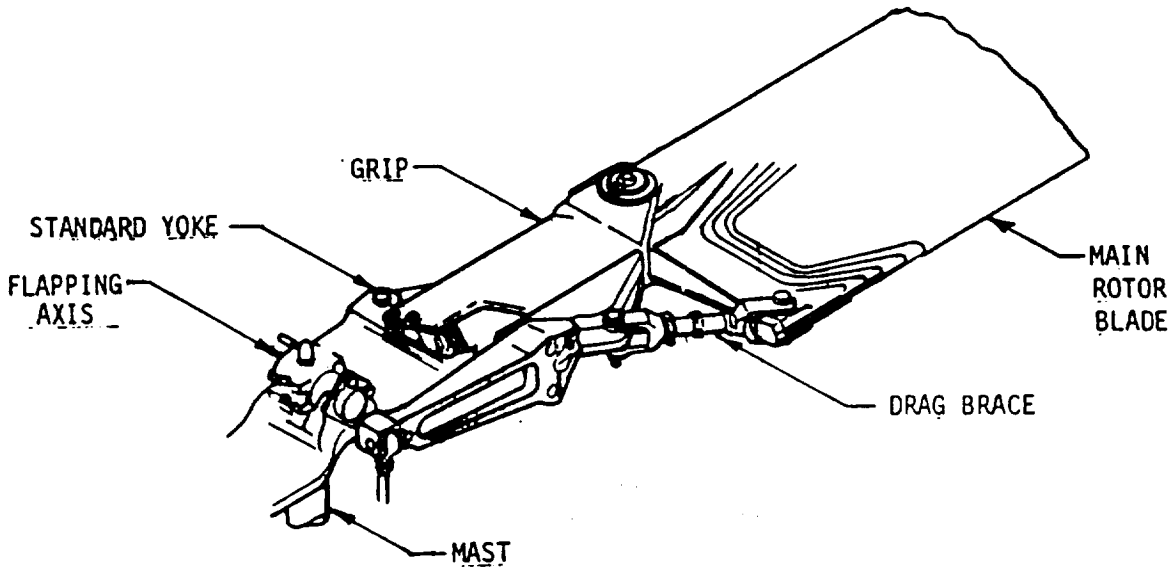

Figure 1.2 Model of a Bell Two Bladed Teetering Rotor

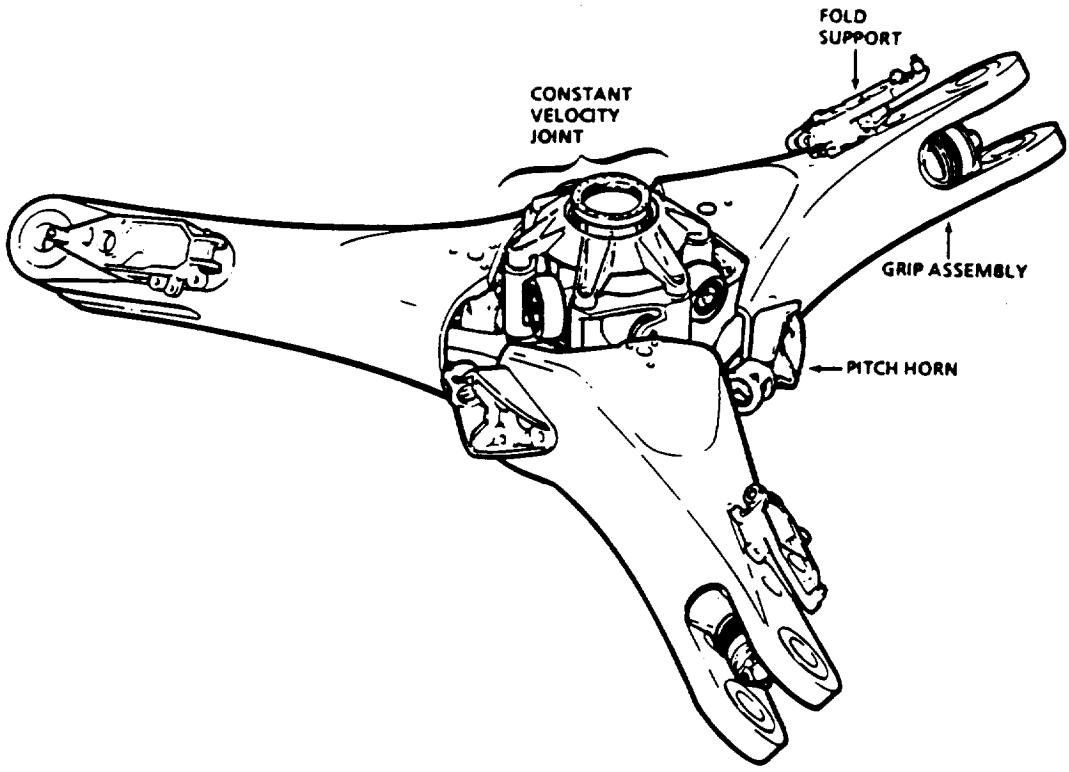

Figure 1.3 Gimballed Rotor Hub

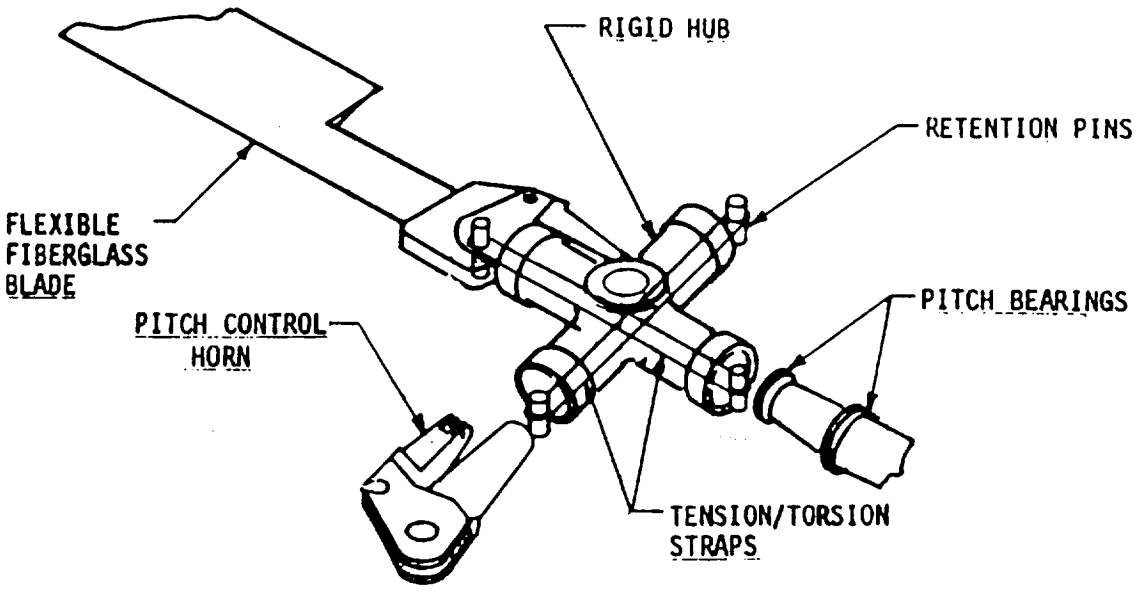

Figure 1.4 Model of a Hingeless Rotor

flying qualities, mechanical simplicity and low maintenance). The recent advances in composite materials make the bearingless rotor a viable concept [30]. The rotor blades in these systems are attached to the hub via composite flexible structural elements known as load paths or branches. These branches accommodate rotor motions by deflecting elastically thereby eliminating the need for hinges.

Conventional helicopter blades are idealized as single–load–path blades and as mentioned earlier the transfer matrix method is a very convenient and efficient method to analyze such single branch structures. All practical designs of bearingless rotors include multiple branches at the root, and the one that was flight tested by Boeing Helicopter Co. has three load branches consisting of two flexbeams and a nonenclosing torque tube [31]. It is shown in Figure 1.5. Now, almost all of the current bearingless rotor designs consist of a single flexbeam with a wrap–around torque tube called a pitch cuff (Figure 1.6).

The goal of this research is to develop the transfer matrix method to treat nonlinear autonomous boundary value problems with multiple branches. The application is the complete nonlinear aeroelastic analysis of multiple-branched rotor blades. Once the development is complete, it can be incorporated into the existing transfer matrix analyses mentioned previously. There are several difficulties to be overcome in reaching this objective. The conventional transfer matrix method is limited in that it is applicable

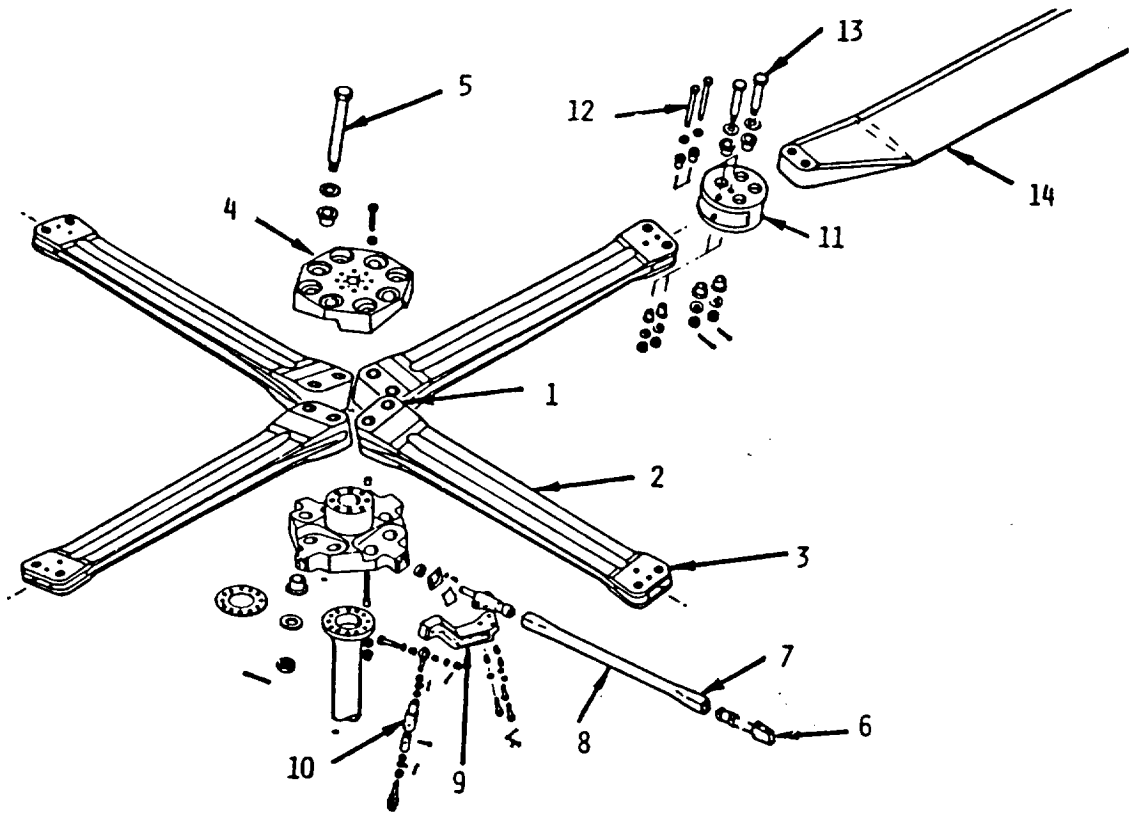

ITEM	DESCRIPTION
1	FLEXURE, INBOARD ATTACHMENT
2	FLEXURE
3	FLEXURE, OUTBOARD ATTACHMENT
4	STEEL HUB
5	FLEXURE/HUB ATTACHMENT BOLTS
6	TORQUE TUBE, OUTBOARD FITTING
7	TORQUE TUBE, OUTBOARD ATTACHMENT
8	TORQUE TUBE
9	PITCH ARM ASSEMBLY
10	PITCH LINK ASSEMBLY
11	CLEVIS
12	TORQUE TUBE/CLEVIS ATTACHMENT BOLTS
13	BLADE/CLEVIS ATTACHMENT BOLTS
14	ROTOR BLADE ASSEMBLY

Figure 1.5 Components of a First Generation Bearingless Rotor

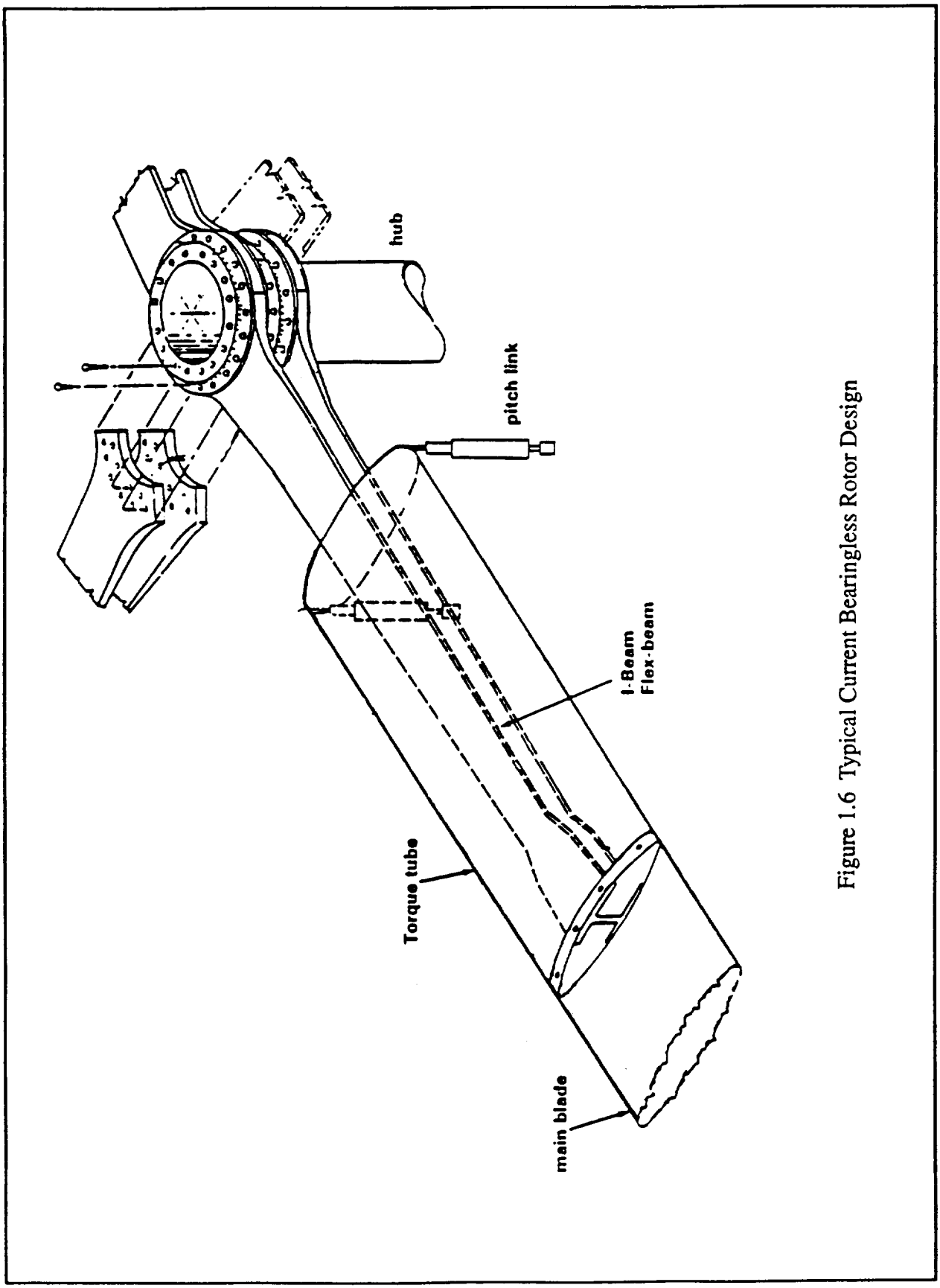

Figure 1.6 Typical Current Bearingless Rotor Design

only to linear single branch chain–like structures, but consideration of multiple branch modeling is important for bearingless rotors [33]. Also, hingeless and bearingless rotor blade dynamic characteristics (particularly their aeroelasticity problems) are inherently nonlinear. Murthy and Joshi [34] have developed a transfer matrix method to determine the natural frequencies and modes of rotor blades with multiple branches at the root. This development was based on linear homogeneous equations of motion. Sangha [35] has described a transfer matrix method to analyze a bearingless multiple–load–path blade.

In the present work the nonlinear equations of motion and the multiple-branched boundary value problem are treated together using a direct transfer matrix method. First, the formulation is applied to a nonlinear single–branch blade to validate the nonlinear portion of the formulation. The nonlinear system of equations is iteratively solved using a form of Newton–Raphson iteration scheme developed for differential equations of continuous systems. The formulation is then applied to determine the nonlinear steady state trim and aeroelastic stability of a rotor blade in hover with two branches at the root. A comprehensive computer program is developed, and is used to obtain numerical results for the (1) free vibration, (2) nonlinearly deformed steady state, (3) free vibration about the nonlinearly deformed steady state and (4) aeroelastic stability tasks. The numerical results obtained by the present method agree with results from other methods.

2. EQUATIONS OF MOTION

2.1 Nonlinear Equations for Elastic Bending and Inertial Loadings

The nonlinear differential equations of motion for the fully coupled elastic flapwise bending, chordwise bending, torsion and axial extension of twisted nonuniform rotor blades are given below. The development of the equations is the subject of reference [36], in which their complete derivation is presented. In addition to the present project, these equations form the basis for structural beam modeling in the current state of the art rotorcraft analysis programs. The equations are valid for any beam, and the mass, elastic and tension axes need not be coincident. The coordinate system they are derived in is an undeformed coordinate system, with x positive outward along the span, y positive towards the leading edge, and z positive upwards (see Figure 2.1). For algebraic conciseness the terms containing e_A, B_1^*, B_2^*, C_1 and C_1^* are treated as zero. It should be noted that this assumption does not affect the general nature of the formulation presented here-in.

Axial Extension:

$$[EA(u'+v'^2/2+w'^2/2)]' + \Omega^2 mu - m\ddot{u} + 2\Omega m\dot{v} = -\Omega^2 mx \qquad (2.1)$$

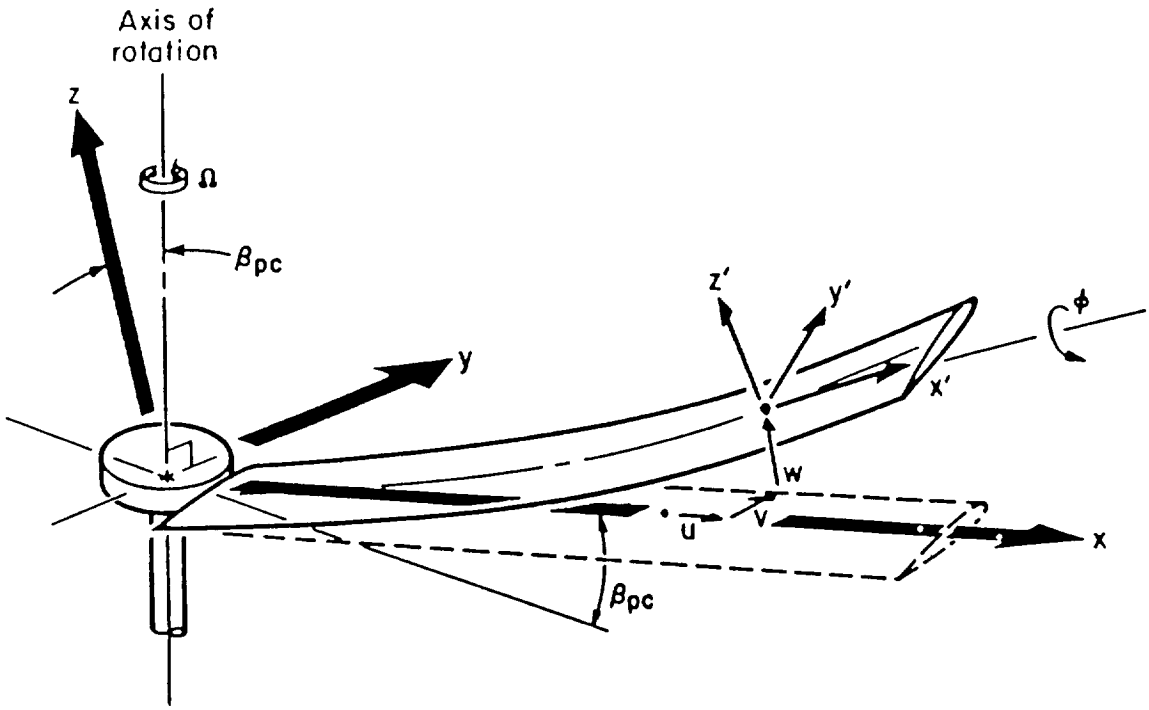

Figure 2.1 Rotor blade deformed (x',y',z') and undeformed (x,y,z) coordinate systems and displacements.

Lead-Lag:

$$
\begin{aligned}
&-(Tv')' + \{(EI_z\cos^2(\theta+\phi) + EI_y\sin^2(\theta+\phi)]v'' \\
&\quad +(EI_z-EI_y)\cos(\theta+\phi)\sin(\theta+\phi)w''\}'' \\
&\quad + 2\Omega m\dot{u} + m\ddot{v} - me\ddot{\phi}\sin\theta - 2me\Omega(\dot{v}'\cos\theta+\dot{w}'\sin\theta) \\
&\quad - m\Omega^2[v+e\cos(\theta+\phi)] - 2m\Omega\beta_{pc}\dot{w} \\
&\quad - \{me[\Omega^2 x\cos(\theta+\phi) + 2\Omega\dot{v}\cos\theta)\}' = L_v
\end{aligned}
\tag{2.2}
$$

Flap:

$$
\begin{aligned}
&-(Tw')' + \{(EI_z-EI_y)\cos(\theta+\phi)\sin(\theta+\phi)]v'' \\
&\quad +(EI_z\sin^2(\theta+\phi) + EI_y\cos^2(\theta+\phi)w''\}'' \\
&\quad + 2m\Omega\beta_{pc}\dot{v} + m\ddot{w} + me\ddot{\phi}\cos\theta \\
&\quad - \{me[\Omega^2 x\sin(\theta+\phi) \\
&\quad + 2\Omega\dot{v}\sin\theta)\}' = L_w - \Omega^2 m\beta_{pc}x
\end{aligned}
\tag{2.3}
$$

Torsion:

$$
\begin{aligned}
&-(GJ+Tk_A^2)\phi']' + (EI_z-EI_y)(w''^2-v''^2)\cos\theta\sin\theta \\
&\quad + v''w''\cos2\theta] + mk_m^2\ddot{\phi} + m\Omega^2\phi(k_{m_2}^2-k_{m_1}^2)\cos2\theta \\
&\quad - me[\Omega^2 x(w'\cos\theta-v'\sin\theta) \\
&\quad - (\ddot{v} -\Omega^2 v)\sin\theta+\ddot{w}\cos\theta] = M_e \\
&\quad - m\Omega^2(k_{m_2}^2-k_{m_1}^2)\cos\theta\sin\theta - me\Omega^2\beta_{pc}x\cos\theta
\end{aligned}
\tag{2.4}
$$

2.2 First Order Equations

Equations (2.1)-(2.4) can be reduced to a system of first-order nonlinear differential equations in terms of the state vector containing deflections and forces [37]. The state vector {Z} is defined as

$$\lfloor u \;\; w \;\; v \;\; \varepsilon \;\; \zeta \;\; \phi \;\; M_x \;\; M_y \;\; M_z \;\; V_y \;\; V_z \;\; V_x \rfloor \tag{2.5}$$

and the governing equations are written in the undeformed coordinate system.

First the differential equations of the three translations u, w and v are developed. From equation (90) of reference [36]

$$V_x' \approx V_x = EA\left(u' + \frac{v'^2}{2} + \frac{w'^2}{2}\right) \tag{2.6}$$

The bending rotations (slopes) are

$$w' = \varepsilon \tag{2.7}$$

$$v' = \xi \tag{2.8}$$

Substitution of equations (2.7) and (2.8) into equation (2.6) gives

$$u' = -\varepsilon^2/2 - \xi,^2/2 + V_x/EA \tag{2.9}$$

Expressions for the bending rotations (ε', ζ', ϕ') are determined as follows. From equations (91), (92) and (96) of reference [36]

$$M_x' = GJ\phi' \tag{2.10}$$

$$M_{z'} = EI_z[v'' \cos(\theta+\phi) + w'' \sin(\theta+\phi)] \tag{2.11}$$

$$M_{y'} = EI_y[v'' \sin(\theta+\phi) - w'' \cos(\theta+\phi)] \tag{2.12}$$

In matrix form, the above equations are

$$\begin{Bmatrix} M_{x'} \\ M_{z'} \\ M_{y'} \end{Bmatrix} = \begin{bmatrix} 0 & 0 & GJ \\ EI_z s\alpha & EI_z c\alpha & 0 \\ -EI_y c\alpha & EI_y s\alpha & 0 \end{bmatrix} \begin{Bmatrix} \phi' \\ \xi' \\ \theta' \end{Bmatrix} \tag{2.13}$$

where s = sine, c = cosine and $\alpha = \theta + \phi$. In transforming these moments to the undeformed coordinate system, the following parameters must be considered. From equation (A6) of [36]

$$\theta + \hat{\phi} + v'w' = \theta + \phi - \int_0^x v''w'dx + v'w'$$

or $$\theta + \hat{\phi} + v'w' = \theta + \phi + \upsilon \tag{2.14}$$

where

$$\upsilon = v'w' - \int_0^x v''w'dx = \int_0^x v'w''dx \tag{2.15}$$

Assuming small υ,

$$\theta + \hat{\phi} + v'w' = \theta + \phi \tag{2.16}$$

Given equation (2.16), equations (3) of [36] relate the bending moments in the deformed coordinate system (x', y', z') to those in the undeformed coordinate system (x,y,z)

$$M_x = M_x' - M_z'(-\zeta s\alpha+\varepsilon c\alpha) - M_y'(\xi c\alpha+\varepsilon s\alpha) \tag{2.17}$$

$$M_z = M_x'\varepsilon + M_z'c\alpha + M_y's\alpha \tag{2.18}$$

$$M_y = M_x'\xi - M_z's\alpha + M_y'c\alpha \tag{2.19}$$

by neglecting ε^2, ξ^2 compared to unity. In matrix form the above equations are

$$\begin{Bmatrix} M_x \\ M_y \\ M_z \end{Bmatrix} = \begin{bmatrix} 1 & +\varepsilon s\alpha - \varepsilon c\alpha & -\xi c\alpha - \varepsilon s\alpha \\ \varepsilon & c\alpha & s\alpha \\ \xi & -s\alpha & c\alpha \end{bmatrix} \begin{Bmatrix} M_x' \\ M_z' \\ M_y' \end{Bmatrix} \tag{2.20}$$

Premultiplication of equation (2.13) by the coefficient matrix of (2.20) results in an expression relating derivatives of rotations to bending moments in the deformed coordinate system. Substituting equation (2.20) into this expression gives

$$\begin{Bmatrix} M_x \\ M_z \\ M_y \end{Bmatrix} = [C] \begin{Bmatrix} \varepsilon' \\ \xi' \\ \phi' \end{Bmatrix} \tag{2.21}$$

where [C] is defined as

$$[C] = \begin{bmatrix} b^2 + b_1\xi & -b_1\xi - b_3\varepsilon & GJ \\ -b_1 & b_3 & GJ\varepsilon \\ -b_2 & b_1 & GJ\xi \end{bmatrix}$$

and

$$\left.\begin{aligned} b_1 &= (EI_y - EI_z)c\alpha s\alpha \\ b_2 &= EI_y c^2\alpha + EI_z s^2\alpha \\ b_3 &= EI_y s^2\alpha + EI_z c^2\alpha \\ b_4 &= b_3 - b_2 \end{aligned}\right\} \qquad (2.22)$$

Inversion of the coefficient matrix [C] in equation (21) and subsequent rearrangement yield the desired differential equations of rotations.

$$\psi' = GJ(b_3\xi - b_1\varepsilon)M_x/D + GJb_1(1+\xi^2+b_3\xi\varepsilon/b_1)M_z/D - GJb_3(1+\varepsilon^2+b_1\xi\varepsilon/b_3)M_y/D \qquad (2.23)$$

$$\xi' = GJ(b_1\xi - b_2\varepsilon)M_x/D + GJb_2(1+\xi^2+b_1\xi\varepsilon/b_2)M_z/D - GJb_1(1+\varepsilon^2+b_2\xi\varepsilon/b_1)M_y/D \qquad (2.24)$$

$$\phi' = (b_3b_2 - b_1^2)M_x/D + b_3b_2 - b_1^2)\varepsilon M_z/D + (b_3b_2 - b_1^2)\xi M_x/D \qquad (2.25)$$

where

$$D = GJ[(b_3b_2 - b_1^2)(1+\xi^2+\varepsilon^2)]$$

and

$$b_3b_2 - b_1^2 - EI_yEI_z$$

In equations (2.23) through (2.25), ξ^2, ε^2 are neglected compared to unity, yielding

$$\varepsilon' = \frac{b_3\xi - b_1\varepsilon}{EI_yEI_z}M_x + \frac{b_1}{EI_yEI_z}M_z - \frac{b_3}{EI_yEI_z}M_y \qquad (2.26)$$

$$\xi' = \frac{b_1\xi - b_2\varepsilon}{EI_yEI_z} M_x + \frac{b_2}{EI_yEI_z} M_z - \frac{b_1}{EI_yEI_z} M_z \tag{2.27}$$

$$\phi' = \frac{M_x}{GJ} + \frac{M_z}{GJ}\varepsilon + \frac{M_y}{GJ}\xi \tag{2.28}$$

Assuming the torsional displacement angle ϕ is small,

$$\left.\begin{aligned} \cos(\theta+\phi) &= \cos\theta - \phi\sin\theta \\ \sin(\theta+\phi) &= \sin\theta + \phi\cos\theta \end{aligned}\right\} \tag{2.29}$$

Substitution of (2.29) into (2.22) gives

$$\left.\begin{aligned} b_1 &= (EI_y - EI_z)(\cos\theta\sin\theta + \phi\cos 2\theta) \\ b_2 &= EI_y(\cos^2\theta - \phi\sin 2\theta) + EI_z(\sin^2\theta + \phi\sin 2\theta) \\ b_3 &= EI_y(\sin^2\theta + \phi\sin 2\theta) + EI_z(\cos^2\theta + \phi\sin 2\theta) \\ b_4 &= b_3 - b_2 \end{aligned}\right\} \tag{2.30}$$

neglecting ϕ^2 terms.

Define

$$\left.\begin{aligned} a_1 &= (EI_y - EI_z)\cos\theta\sin\theta/EI_yEI_z \\ a_2 &= \cos^2\theta/EI_z + \sin^2\theta/EI_y \\ a_3 &= \sin^2\theta/EI_z + \cos^2\theta/EI_y \\ a_4 &= a_3 - a_2 \end{aligned}\right\} \tag{2.31}$$

Then from equation (2.30) and (2.31) let

$$\left.\begin{aligned} b_1/EI_yEI_z &= a_1 - a_4\phi \\ b_2/EI_yEI_z &= a_2 - 2a_1\phi \\ b_3/EI_yEI_z &= a_3 + 2a_1\phi \\ b_4/EI_yEI_z &= a_4 \end{aligned}\right\} \qquad (2.32)$$

Substituting equation (2.32) into the relations (2.26), (2.27) and (2.28) for ε', ξ' and ϕ', and neglecting third order nonlinear terms yields

$$\varepsilon' = (a_3\xi - a_1\varepsilon)M_x + (a_1 - a_4\phi)M_z - (a_3 + 2a_1\phi)M_y \qquad (2.33)$$

$$\xi' = (a_1\xi - a_2\varepsilon)M_x + (a_2 - 2a_1\phi)M_z - (a_1 - a_4\phi)M_y \qquad (2.34)$$

$$\phi' = M_x/GJ + M_z\varepsilon/GJ + M_y\xi GJ \qquad (2.35)$$

The first order differential equations for the moments are developed from equations of equilibrium (68) of inertial moments (88) of [36].

$$\begin{aligned} \frac{dM_x}{dx} = {} & V_y\varepsilon - V_z\xi - m\{e[(\ddot{v} - \Omega^2 v)(\sin\theta + \phi\cos\theta) \\ & - \ddot{w}(\cos\theta + \phi\sin\theta) + 2\Omega\dot{u}\sin\theta - \Omega^2 x\beta_{pc}\cos\theta] - k_m^2\ddot{\phi} \\ & - \Omega^2(k_{m_2}^2 - k_{m_1}^2)(\cos\theta\sin\theta) + \phi\cos 2\theta - \phi^2\cos\theta\sin\theta) \\ & -2\Omega[(k_{m_2}^2 - k_{m_1}^2)\xi\sin\theta\cos\theta \\ & + \dot{\varepsilon}(k_{m_2}^2\sin^2\theta + k_{m_1}^2\cos^2\theta)]\} - M_e \end{aligned} \qquad (2.36)$$

where M_e is the aerodynamic pitching moment about the elastic axis

$$\frac{dM_z}{dx} = -V_y + V_x\xi + me[\Omega^2 x(\cos\theta - \phi\sin\theta) + 2\Omega\dot{v}\cos\theta] \qquad (2.37)$$

$$\frac{dM_y}{dx} = V_z + V_x\varepsilon - me[\Omega^2 x(\sin\theta+\phi\cos\theta) + 2\Omega\dot{v}\sin\theta] \qquad (2.38)$$

The first order differential equations for the forces are developed from equations of equilibrium (69) of [36] and inertial forces given by equation (87) of [36].

$$\frac{dV_y}{dx} = m\{\ddot{v} - e\ddot{\phi}\sin\theta - \Omega^2[v + e(\cos\theta-\phi\sin\theta)] + 2\Omega[\dot{u} - e\{\dot{\xi}\cos\theta+\dot{\epsilon}\sin\theta)]\} - L_v - 2m\Omega\beta_{pc}\dot{w} \qquad (2.39)$$

where L_v is the aerodynamic force acting in the y direction positive towards the leading edge

$$\frac{dV_z}{dx} = m(\ddot{w} - e\ddot{\phi}\cos\theta) - L_w + 2m\Omega\beta_{pc}\dot{v} + m\beta_{pc}\Omega^2 x \qquad (2.40)$$

where L_w is the aerodynamic force acting in the z (upward) direction.

$$\frac{dV_x}{dx} = m\Omega^2(x+u) - 2\Omega m\dot{v} + m\ddot{u} \qquad (2.41)$$

Thus equations (2.9), (2.7), (2.8) and (2.33) through (2.41) are the desired first order nonlinear differential equations governing the

state vector. The aerodynamic loadings, L_v, L_w and M_e are evaluated next.

2.3 Aerodynamics

Helicopter rotors typically operate in a complex aerodynamic environment. During one revolution (typically 1/5 of a second) the blade can experience large variations in angle of attack and Mach number, unsteady aerodynamic effects and stall effects.

To model the rotor aerodynamic environment, lifting line or lifting surface theories can be employed. Lifting line technology is a more mature technology and for that reason is used extensively in the helicopter industry.

The rotating blade is modeled as a rotating lifting line. Strip theory is then applied to this lifting line, resulting in a finite number of discrete bound vortex segments representing airfoil sections. Unsteady aerodynamic theory has been developed for the lifting line approximation of a fixed wing in references [37] and [39]. Unsteady aerodynamics takes the complete vortex system into account and gives rise to two classes of forces - circulatory and noncirculatory. The circulatory forces are a consequence of the vorticity (bound and trailed). The noncirculatory forces (sometimes referred to as virtual or apparent forces) are not due to vorticity. Lift may be expressed as the sum of its circulatory and noncirculatory components.

$$L_{Total} = L_{Circulatory} + L_{Noncirculatory} \tag{2.42}$$

Theodorsen noted in [37] that if a wing was undergoing pure harmonic motion at frequency ω, the wake vorticity was periodic and subsequently circulatory lift would be also. The Theodorsen lift deficiency function C(k) thus modifies the circulatory lift. It accounts for the effect of shed vorticity in the wake and subsequent time varying lift build up on the wing.

$$L_{Total} = C(k)L_{Circulatory} + L_{Noncirculatory} \tag{2.43}$$

where k is a reduced frequency, given by

$$k = \frac{\omega b}{U} \tag{2.44}$$

The magnitude of C ranges from .5 at high frequency to 1. at low frequency, and thus usually reduces the circulatory lift. The phase of C represents the delay (or lag) in the lift build up. The magnitude and phase of C(k) are shown in Figure 2.2. There are different levels of approximations for unsteady aerodynamics, and usually they are divided into the following three categories.

(i) Complete Unsteady Aerodynamics

The complete theory is employed to represent the unsteady effects of the shed vorticity, and includes circulatory and noncirculatory forces.

$$L_{Total} = C(k)L_{Circulatory} + L_{Noncirculatory} \tag{2.45}$$

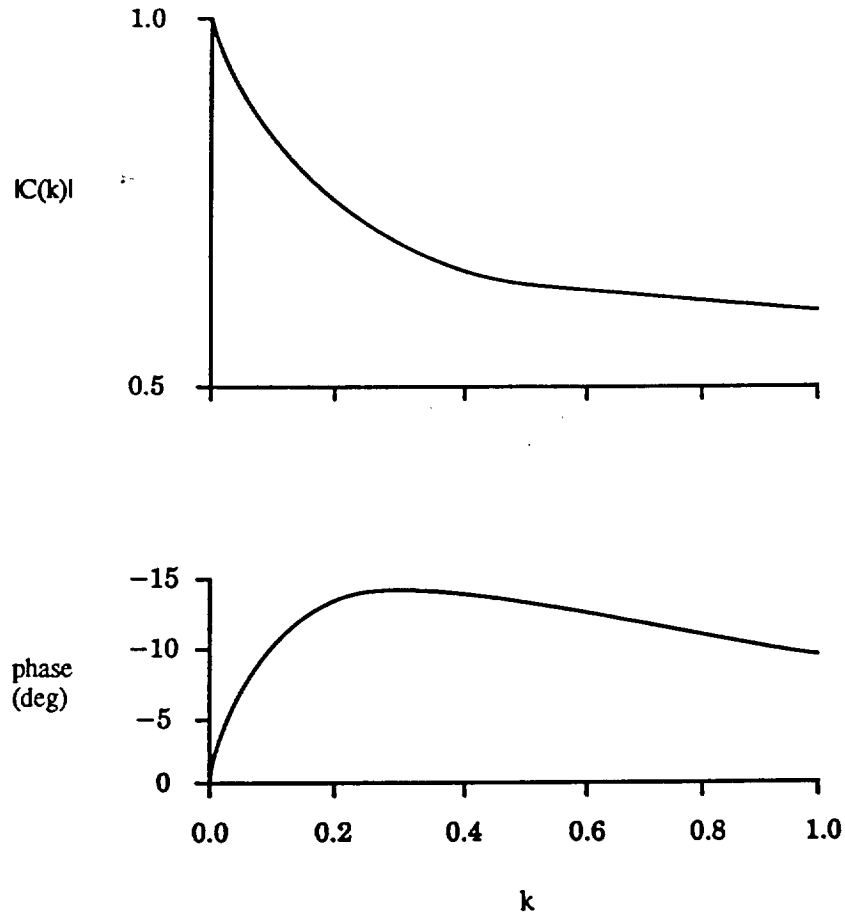

Figure 2.2 Theodorsen Lift Deficiency Function, C(k)

The results obtained correspond to characteristic frequencies of approximately 40 cycles per second.

(ii) Quasi-Unsteady Aerodynamics

In this instance the noncirculatory terms are neglected.

$$L_{Total} = C(k)L_{Circulatory} \tag{2.46}$$

The theory yields satisfactory results for frequencies between 5 and 15 cycles/sec,

(iii) Quasi-Steady Aerodynamics

$$L_{Total} = L_{Circulatory} \tag{2.47}$$

This approximation is generally used at charactreristic frequencies which are on the order of 1 cycle per second. It neglects the effect of wake vortices on the flow field, but unsteady rotor motions still produce an unsteady downwash. This unsteady downwash is employed to establish the bound circulation by satisfying the tangency boundary condition.

In the present formulation the quasi-steady aerodynamics are employed because the aeroelastic instabilities under investigation are quite low. (In hover the reduced frequency is small, so C(k) = 1 and negligible phase lag is a good approximation. As forward speed

is increased, the reduced frequency also increases. For increasing k, C(k) is a value <1.0 (as can be seen in Figure 2.2) and the accuracy of the approximation is somewhat reduced although it is still useful.)

2.3.1 Airloads

The quasi-steady lift and moment coefficients about the mid chord point are given by [39] as

$$C_l^{qs} = 2 \int_{-1}^{1} \sqrt{\frac{1-\xi^*}{1+\xi^*}}\, w(\xi^*) d\xi^* \tag{2.47}$$

$$C_{m_{c/2}}^{qs} = C_l^{qs} + 2 \int_{1}^{-1} \sqrt{\frac{1-\xi^*}{1+\xi^*}}\, \xi^* \sqrt{\frac{w(\xi^*)}{U}}\, d\xi^* \tag{2.48}$$

where the downwash velocity is

$$w(y,t) = \frac{\rho z_a}{\rho t} - U \frac{\rho z_a}{\rho y} \tag{2.49}$$

and

$$C_l^{qs} = l^{qs}/\rho U^2 b$$

$$C_m^{qs} = m^{qs}/\rho U^2 b^2$$

The equation for the meanline of a thin airfoil which is free to translate vertically and pitch about the mid-chord is given by (see Figure 2.3)

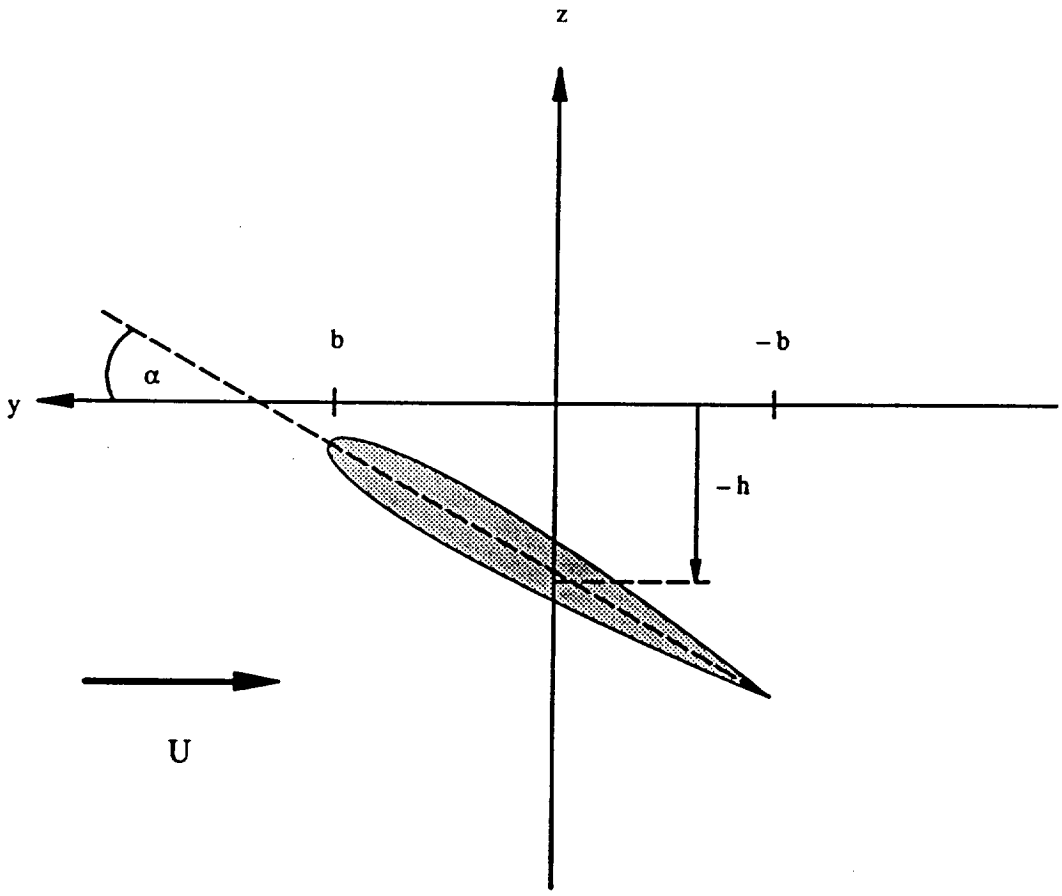

Figure 2.3. Airfoil in Vertical Translation and Pitch About the Mid-Chord

$$z_a(y,t) = h_{c/2} + \tan \alpha y \tag{2.50}$$

From equation (2.49), assuming small α the downwash velocity is given by

$$w(y,t) = \dot{h}_{c/2} - \dot{\alpha} y - \dot{U}\alpha$$

Nondimensionalizing with respect to semi-chord b yields

$$w(\bar{y},t) = \dot{h}_{c/2} - U\alpha + b\dot{\alpha}\bar{y} \tag{2.51}$$

Equation (2.51) is then substituted into the expressions for quasi-steady lift and moment (2.47) and (2.48). The resulting equations may then be integrated with respect to $\bar{y}$ with the help of the integrals in Appendix A.

$$C_l^{qs} = \frac{2\pi}{U}\left(-\dot{h}_{c/2} + U\alpha + \frac{b}{2}\dot{\alpha}\right) \tag{2.52}$$

$$C_{m_{c/2}}^{qs} = \frac{\pi}{U}\left(-\dot{h}_{c/2} + U\alpha\right) \tag{2.53}$$

Traditionally the coefficients are referred to the quarter chord location (also the approximate aerodynamic center). The following equations relate the airloads of mid-chord and quarter-chord and are obtained from the geometry of Figure 2.4.

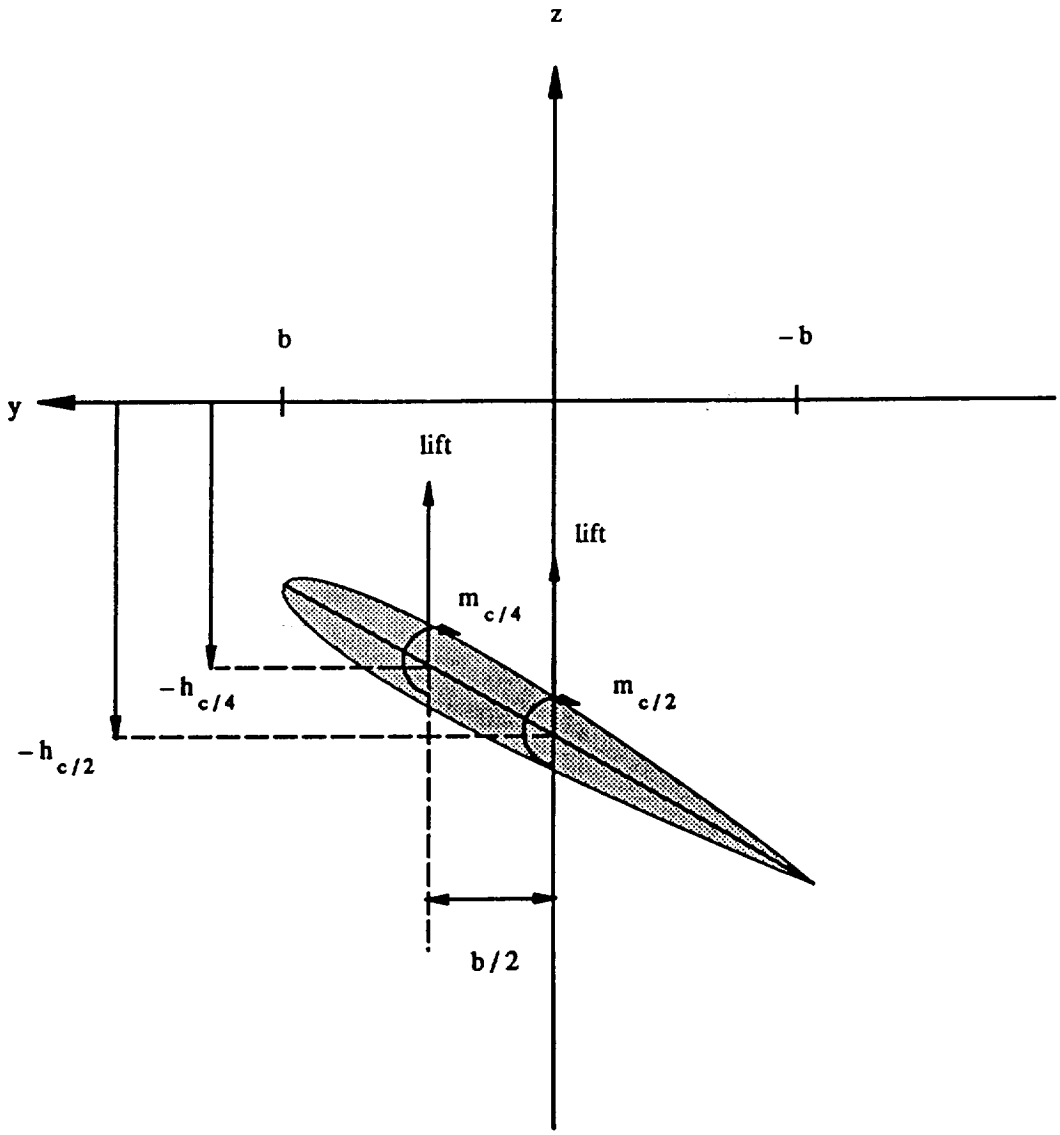

Figure 2.4. Displacement Relations; Mid-Chord to Quarter-Chord

$$\left.\begin{aligned} l &= l_{c/4} = l_{c/2};\ \alpha = \alpha_{c/4} = \alpha_{c/2} \\ h_{c/2} &= h_{c/4} - \alpha b/2 \\ m_{c/2} &= m_{c/4} + lb/2 \end{aligned}\right\} \qquad (2.54)$$

Substitution of equations (2.52) and (2.53) into equation (2.54) and noting the thin airfoil theory theoretical result that 'a' (lift curve slope) equals 2π yields the two dimensional section airloads

$$l = \rho U\alpha(-\dot{h}_{c/e} + U\alpha + b\dot{\alpha} \qquad (2.55)$$

$$m_{c/4} = -\rho bU\alpha\ (\frac{b}{2})^2\ \dot{\alpha} \qquad (2.56)$$

Consider the airfoil to have properties such that the shear center (elastic axis) is not coincident with the quarter-chord location. When the airfoil is plunging and pitching about the shear center as shown in Figure 2.5, the following relations may be written

$$\left.\begin{aligned} h_{c/4} &= h_e + \alpha e\, b \\ m_{c/4} &= m_e - le b \end{aligned}\right\} \qquad (2.57)$$

Obtain l and m_e with respect to the elastic axis (or shear center) (consistent with the nonlinear equations of motion for elastic bending). Substitution of equations (2.55) and (2.56) into equation (2.57) and replacement of b by c/2 yields

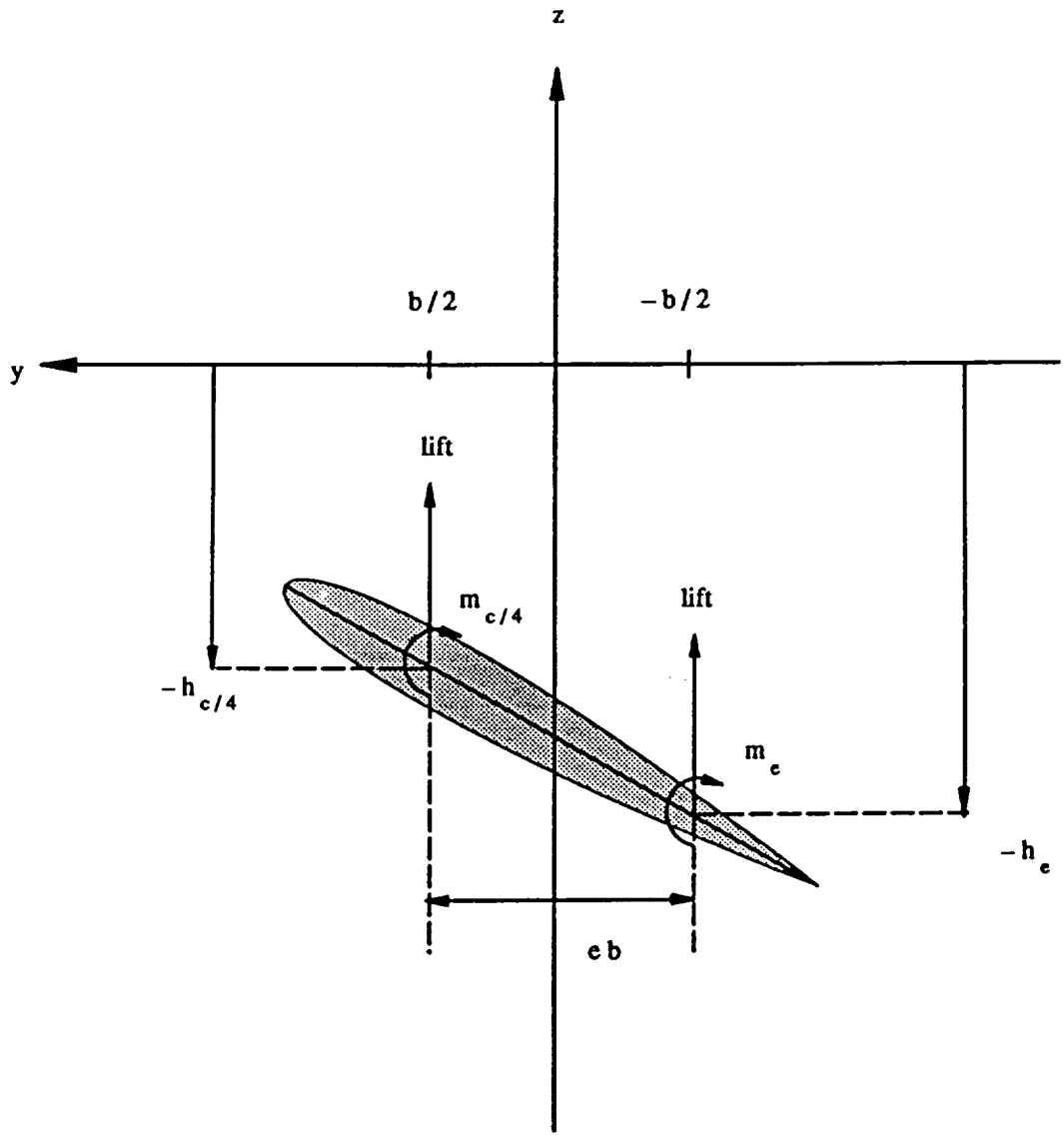

Figure 2.5. Displacement Relations; Quarter-Chord to Shear Center (Elastic Axis)

$$l = \frac{\rho a c}{2} U\{-\dot{h}_e + U\alpha + \frac{c}{2}(1-e)\dot{\alpha}\} \tag{2.58}$$

$$m_e = \frac{\rho a c}{2} U(\frac{c}{4})^2 \{\frac{8e}{c}(-\dot{h}_e + U\alpha) + \dot{\alpha}(4e-e^2-1\} \tag{2.59}$$

Ultimately it is desired to express l and m_e in terms of elastic deflections, and induced and angular velocities. Towards this end, consider a two dimensional airfoil in unsteady motion as shown in Figure 2.6, noting that U is shown opposite to the free stream direction to show it as the airfoil motion. Assuming $\cos\alpha = 1$ and $\sin\alpha = \alpha$ the following expressions for the velocities along the y', z' axes can be written

$$U \approx U_T \tag{2.60}$$

$$U_P \approx \dot{h}_e - U\alpha \tag{2.61}$$

From Appendix A of reference [40], the velocity components can be written as

$$U_T = \Omega x + \dot{v} \tag{2.62}$$

$$U_P = -\Omega x(\theta+\phi+\upsilon) - (\theta+\phi)\dot{v} + v_i + \dot{w} + \Omega v x(\varepsilon+\beta_{pc}) \tag{2.63}$$

$$\dot{\alpha} + \Omega(\varepsilon+\beta_{pc}) \tag{2.64}$$

where

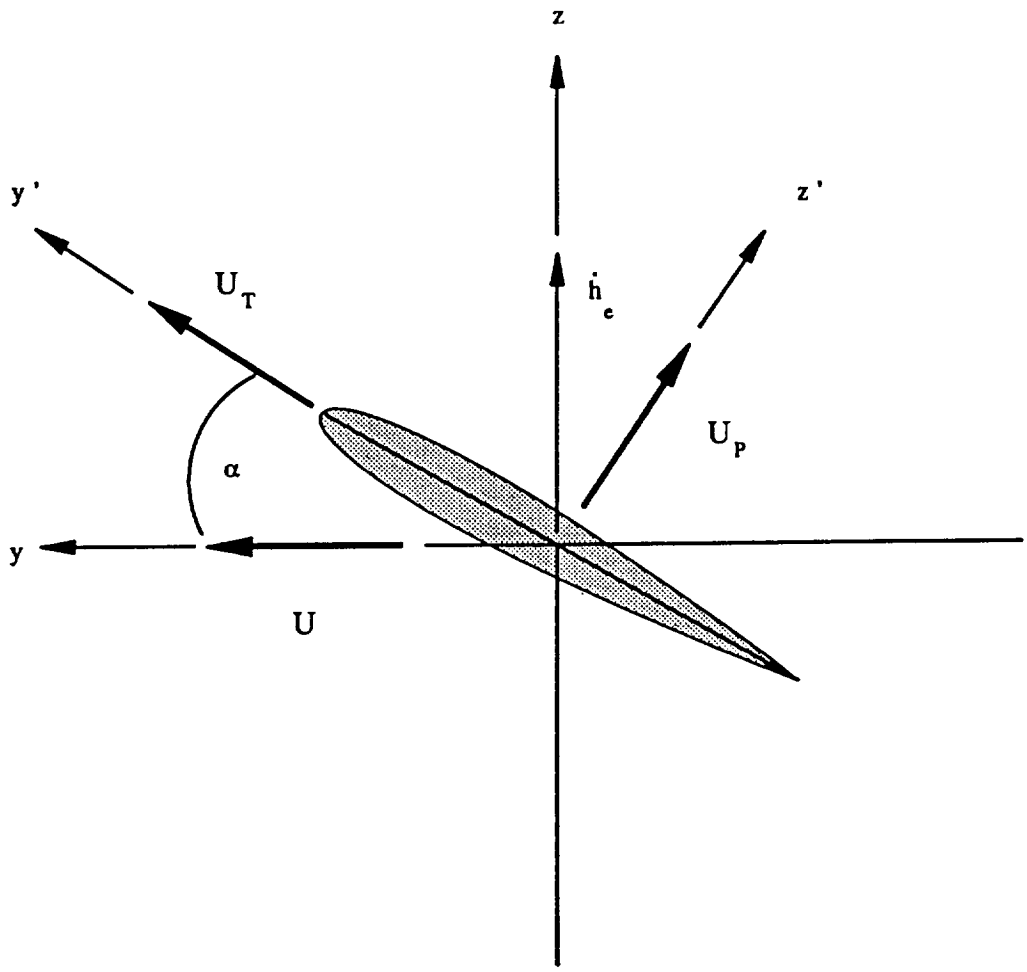

Figure 2.6. Airfoil In Unsteady Motion

$$\upsilon = \int_{o}^{x} \xi\varepsilon' dx \quad = \quad \text{nonlinear angle-of-attack term due to bending} \tag{2.65}$$

Knowing the aerodynamic loadings at the correct location along the chord line (i.e. at the shear center), resolve the airloads from the wind axes back to the undeformed structural axis coordinate system. Consider the aerodynamic loadings acting on the airfoil shown in Figure 2.7. Resolving loadings into components T and S along the deformed (x',y',z') coordinate system axes local to the airfoil gives

$$T = l\cos\alpha + d\sin\alpha \tag{2.66}$$

$$S = l\sin\alpha + d\cos\alpha \tag{2.67}$$

where d is the profile drag given by

$$d = \frac{1}{2}\rho U^2 c_d \tag{2.68}$$

and l is given by equation (2.58). From the geometry of Figure 2.6

$$\cos\alpha = U_T = \sqrt{U_P^2 + U_T^2} \approx U_T/U \tag{2.69}$$

$$\cos\alpha = -U_P = \sqrt{U_P^2 + U_T^2} \approx U_T/U \tag{2.70}$$

since

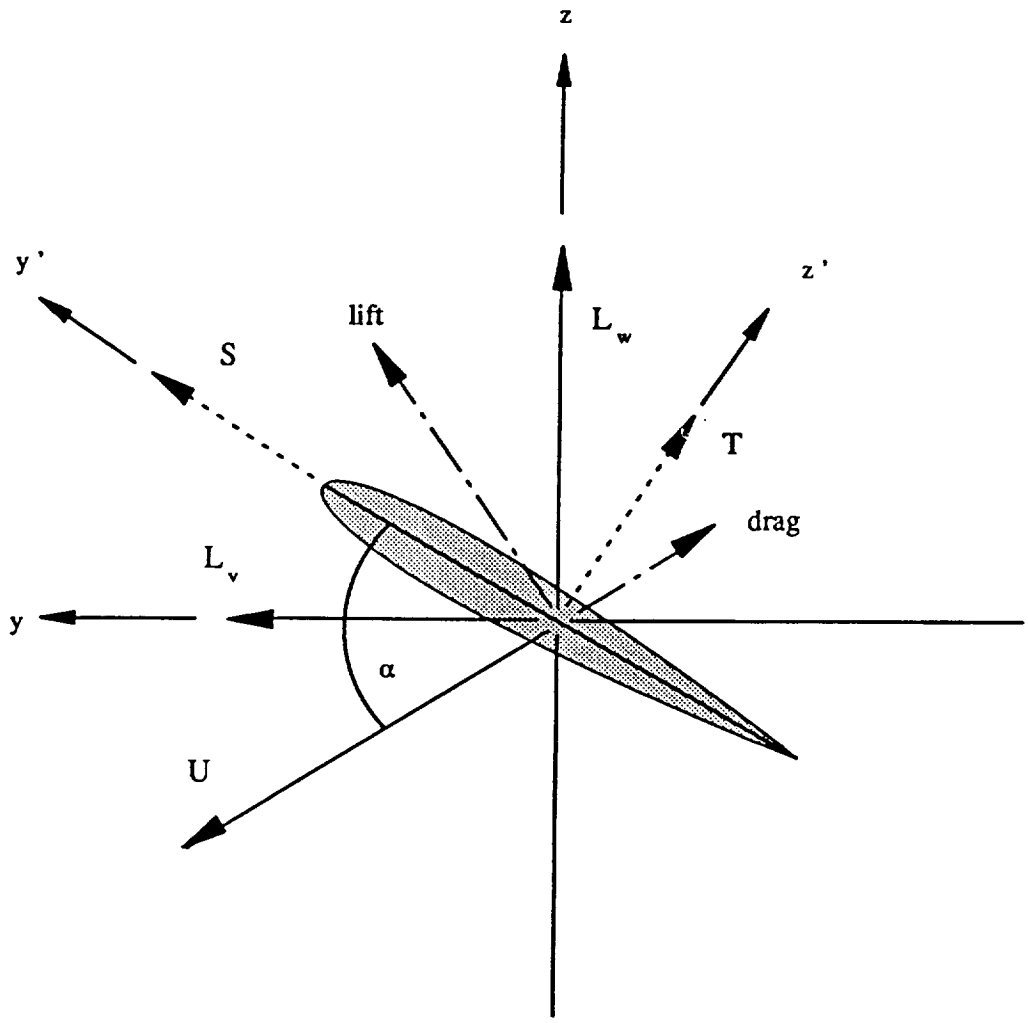

Figure 2.7. Aerodynamic Forces Resolution

$$U = \sqrt{U_T^2 + U_P^2} \tag{2.71}$$

Substituting the equations for section lift and drag (2.58), (2.68) and (2.69) through (2.71) into equations (2.66), (2.67) and (2.59) gives airloads in the deformed coordinate system (x',y',z') as follows.

$$T = \frac{\rho ac}{2}\{-U_P U_T + \frac{c}{2}(1-e)U_T\dot{\alpha}\} \tag{2.72}$$

$$S = \frac{\rho ac}{2}\{-U_P^2 - \frac{c}{2}(1-e)U_P\dot{\alpha} - \frac{cd}{a}U_T^2\} \tag{2.73}$$

Assuming that the resultant airfoil velocity V is approximately equal to the freestream velocity U in Figure 2.7, $\alpha \approx \beta + \phi$ is small. The aeodynamic forces may be referred to the undeformed coordinate system (x,y,z) used to derive the nonlinear elastic bending equations so that they can be incorporated as forcing functions into the differential equations of motion of the system.

$$L_v = S - T(\beta+\phi) \tag{2.74}$$

$$L_w = S(\beta+\phi) + T \tag{2.75}$$

Substitution of equations (2.62) through (2.65), (2.58), (2.72) and (2.73) into equations (2.59), (2.74), and (2.75) yields the following equations for the aerodynamic forces.

$$L_v = \frac{\rho ac}{2}\,[v_i^2 - \Omega^2 x^2 k_2 - \Omega x v_i(\theta+\phi)$$
$$- \{2\Omega x k_2 + (\theta+\phi)v_i\}\dot{v} + \{2v_i - \Omega x(\theta+\phi)\dot{w}$$
$$- k_1\dot{\phi}v_i - k_1\Omega v_i(\varepsilon+\beta_{pc}) - \Omega k_1\dot{w}(\varepsilon+\beta_{pc})] \qquad (2.76)$$

$$L_w = \frac{\rho ac}{2}\,[-\Omega x v_i + \Omega^2 x^2(\theta+\phi+\upsilon) - \Omega^2 x v(\varepsilon+\beta_{pc}) + \Omega^2 x k_1(\varepsilon+\beta_{pc})$$
$$- \{\Omega k_1(\varepsilon+\beta_{pc}) + \Omega x(\theta+\phi) - v_i\}\dot{v}$$
$$- \Omega x\dot{w} + k_1\Omega x\dot{\phi}] \qquad (2.77)$$

$$M_e = k_3 L_w - \frac{\rho ac}{2}\frac{c^2}{16}\{\Omega x\dot{\phi} + \Omega^2 x(\varepsilon+\beta_{pc}) + \Omega\dot{v}(\varepsilon+\beta_{pc})\} \qquad (2.78)$$

where

$k_1 = c(1-e)/2$

$k_2 = c_d/a$

$k_3 = ce/2$

The following assumptions are made in the simplification process leading to equations (2.76) through (2.78).

1. All third order nonlinear terms are dropped.
2. $u, v, w, \psi, \xi, \phi, \dot{u}, \dot{v}, \dot{w}, \dot{\varepsilon}, \dot{\xi}, \dot{\phi}, \theta, \beta_{pac}, v_i$ and k_2 are assumed to be small. Observe θ is not assumed to be small for elastic and inertial forces, but is assumed to be small for the aerodynamics.
3. All nonlinear terms in $\dot{u}, \dot{v}, \dot{w}, \dot{\varepsilon}, \dot{\xi}, \dot{\phi}$ are dropped.

The induced velocity is computed as shown below.

2.3.2 Induced Velocity Model

The induced velocity is computed from the combined momentum and blade-element theory as given by the following equation (reference 41).

$$v_i = \Omega R \left[\frac{-a\sigma_r}{16} + \sqrt{\left(\frac{-a\sigma_r}{16}\right)^2 + \frac{a\sigma_r}{16}\frac{2r}{R}(\theta+\phi)} \right] \qquad (2.79)$$

Note that it is apparent from equations (2.76) through (2.79) that the shear center need not coincide with the aerodynamic center at the quarter chord point.

3. BRANCHED BLADES

Bearingless rotors feature blades connected to a hub via multiple branches. Each branch is designed to react a specific component of load developed by the rotor blade. Flexbeams are soft in torsion, but stiff in bending. They react in and out-of-plane bending moments and centrifugal loadings. Torque tubes or pitch cuffs (which are aerodynamic fairings enclosing the flexbeams) are soft in bending but stiff torsionally; they are used to control the blade in pitch.

A schematic diagram of a multiply branched blade is shown in Figure 3.1. The three branches are connected to the blade through a rigid clevis. The inboard end of the branches are shown clamped. However, the formulation is flexible enough to handle any other root and intermediate clevis conditions.

For the analysis of branched structures by the transfer matrix method, it is important to establish the equilibrium and compatibility relations across the clevis.

3.1 Equilibrium Across the Clevis

The plane of the clevis is shown in Figure 3.2 where h_y^i and h_z^i are the y and z locations of the i^{th} branch from the location of the blade (point 0). The free-body diagram for this clevis is shown in Figure 3.3. Force and moment equilibrium across the clevis yield the following equations:

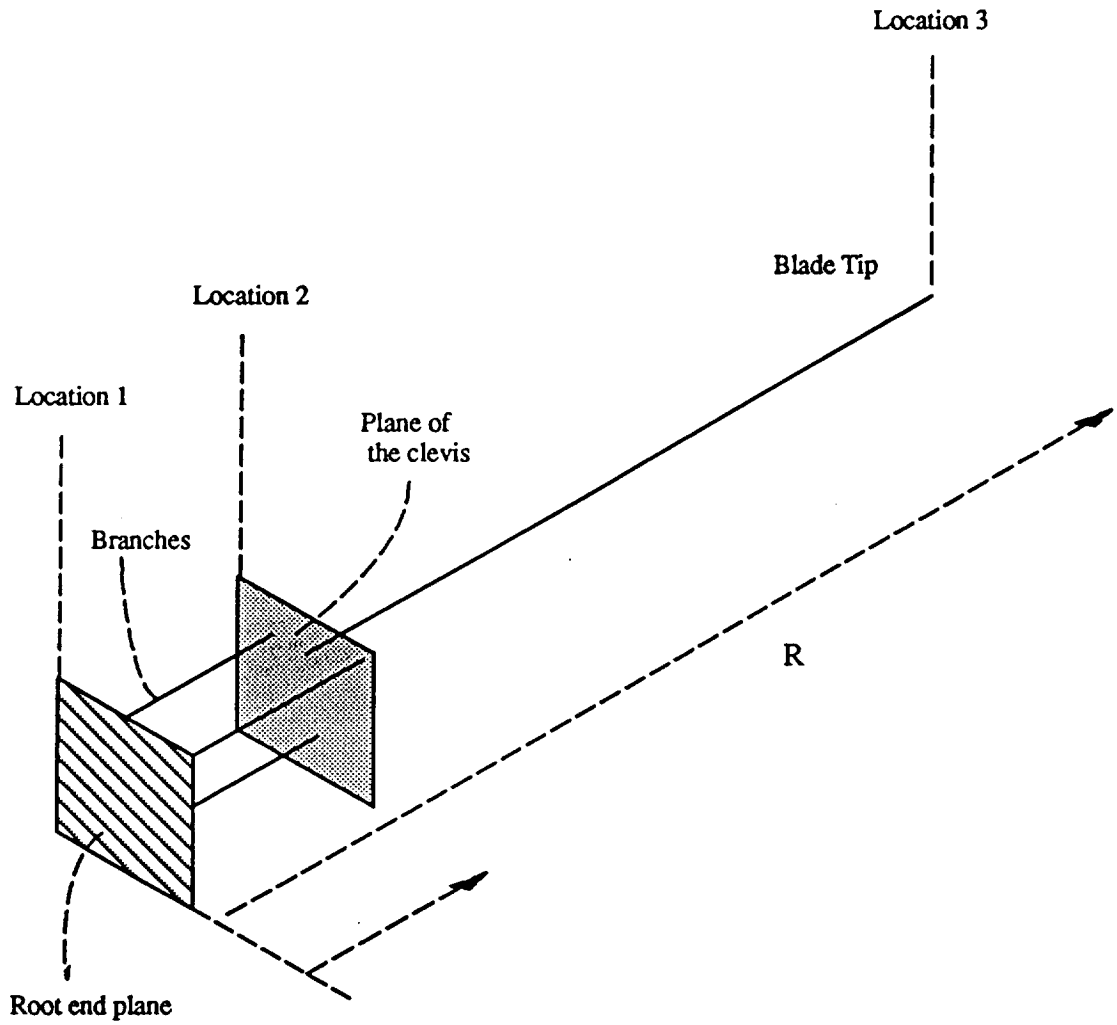

Figure 3.1. Schematic Drawing of a Three Branched Blade

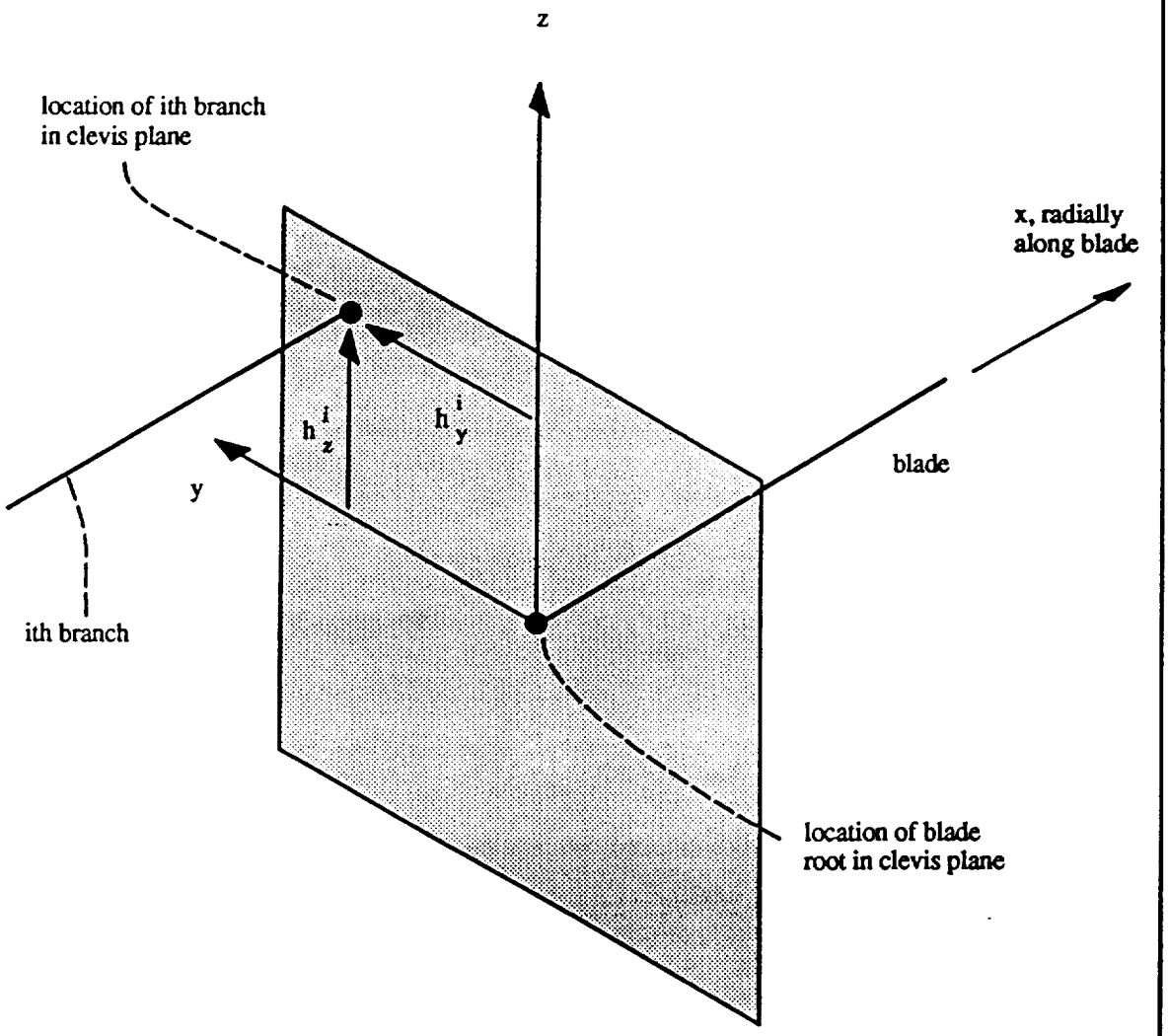

Figure 3.2. Geometry in the Plane of the Clevis

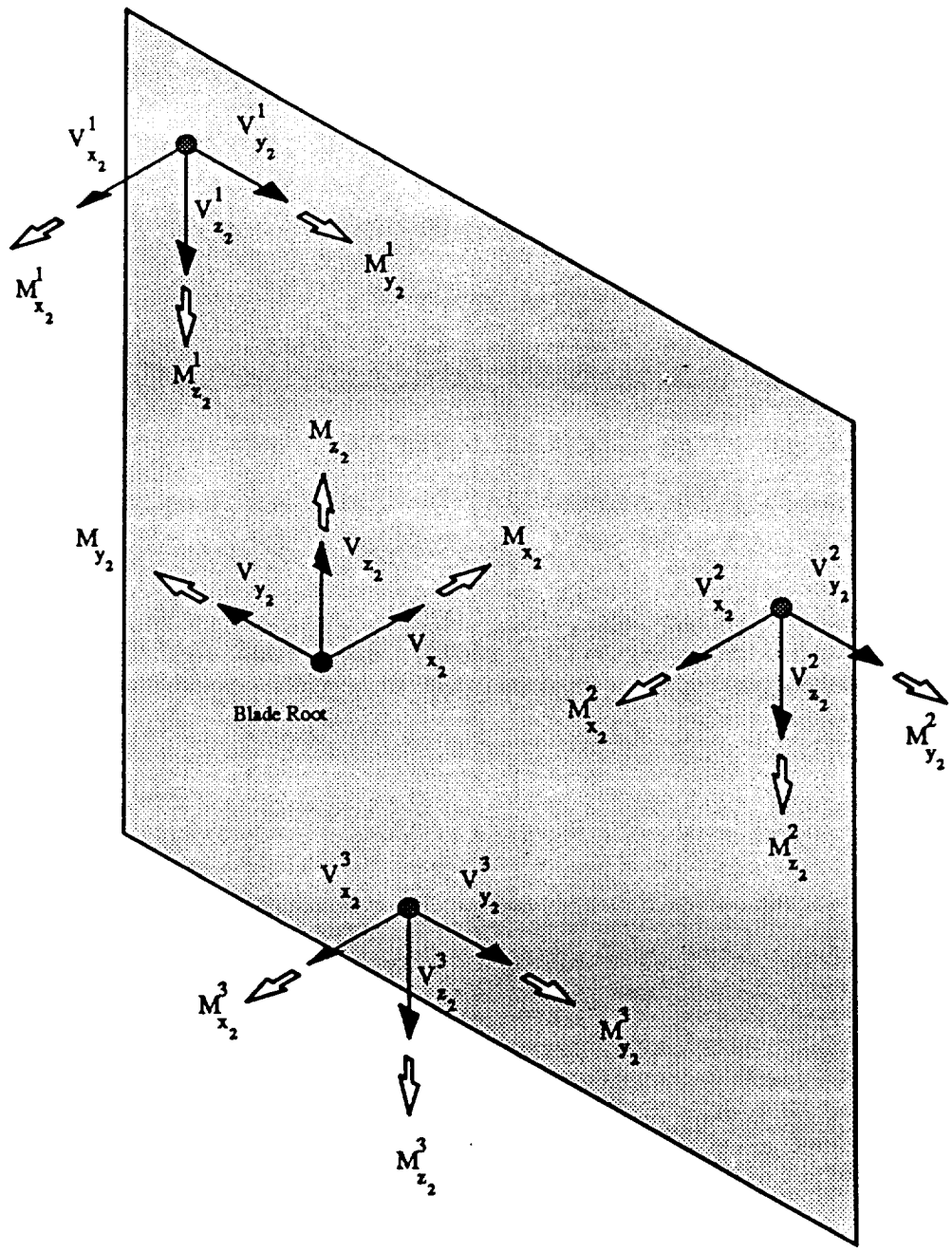

Figure 3.3. Free Body Diagram of the Clevis Plane
● Branch Tip , ● Blade Root

$$
\left.
\begin{aligned}
V_{x_2} &= \sum_{i=1}^{n} V_{x_2}^{i} \\
V_{y_2} &= \sum_{i=1}^{n} V_{y_2}^{i} \\
V_{z_2} &= \sum_{i=1}^{n} V_{z_2}^{i} \\
M_{x_2} &= \sum_{i=1}^{n} \left(M_{x_2}^{i} + h_y^{i} V_{z_2}^{i} - h_z^{i} V_{y_2}^{i} \right) \\
M_{y_2} &= \sum_{i=1}^{n} \left(M_{y_2}^{i} + h_z^{i} V_{x_2}^{i} \right) \\
M_{z_2} &= \sum_{i=1}^{n} \left(M_{z_2}^{i} - h_y^{i} V_{x_2}^{i} \right)
\end{aligned}
\right\} \qquad (3.1)
$$

where n = number of branches.

The above equations can be arranged into a matrix form as shown below:

$$\{f_2\} = \sum_{i=1}^{n} [A^i] \{f_2^i\} \qquad (3.2)$$

where

$$\{f_2\} = \lfloor M_x \quad M_z \quad M_y \quad V_y \quad V_z \quad V_x \rfloor$$

$$[B^i] = \begin{bmatrix} & | & h_z^i & h_y^i & 0 \\ [I] & | & 0 & 0 & -h_{y_i} \\ & | & 0 & 0 & h_z^i \\ - - - & | & - - - - - - - - - - - - - - - \\ [0] & | & & [I] & \end{bmatrix}$$

[I] = Identity matrix

[0] = Null matrix

3.2 Compatibility Across the Clevis

Since the clevis is assumed to be rigid, the displacements and rotations of the branches and the blade are related as shown below (see Figures 3.1 and 3.2)

$$\left.\begin{aligned} u_2 &= u_2^i + h_z^i \varepsilon_2 + h_y^i \xi_2 \\ w_2 &= w_2^i - h_y^i \phi_2^i \\ v_2 &= v_2^i + h_z^i \phi_2^i \\ \varepsilon_2 &= \varepsilon_2^i \\ \xi_2 &= \xi_2^i \\ \phi_2 &= \phi_2^i - \theta_{rc} \end{aligned}\right\} \qquad (3.3)$$

where θ_{rc} = root collective pitch. The above compatibility equations can be arranged into a matrix form as shown below:

$$\{d_2\} = [B^i]\,\{d_2^i\} + \{b\} \qquad (3.4)$$

where

$$\{d_2\}^T = \lfloor \; u \quad w \quad v \quad \varepsilon \quad \xi \quad \phi \; \rfloor$$

$$\{b\}^T = \lfloor \; 0 \quad 0 \quad 0 \quad 0 \quad 0 \quad \theta_{rc} \; \rfloor$$

$$[B^i] = \begin{bmatrix} & | & h_z^i & h_y^i & 0 \\ [I] & | & 0 & 0 & -h_{y_i} \\ & | & 0 & 0 & h_z^i \\ - - - & | & - - - - - - - - - - - - - \\ [0] & | & & [I] & \end{bmatrix}$$

4. NONLINEAR STEADY STATE DEFLECTIONS

4.1 Equations of Motion

Substitution of the aerodynamic forcing functions (equations (2.76)-(2.79) into the twelve governing first order equations (2.7), (2.8), (2.9) and (2.33)-(2.41) yields a set of time dependent nonlinear differential equations. The time dependent terms are dropped to compute the nonlinear steady state deflections, and the resulting equations are given below in matrix form.

$$\{z(x)\}' = [A(x,z)]\ \{z(x)\} + \{f\} \qquad (4.1)$$

where the state vector consists of deflections, slopes, moments and shears.

$$\{z(x)\}^T = \lfloor u\ v\ w\ \varepsilon\ \xi\ \phi\ M_x\ M_z\ M_y\ V_y\ V_z\ V_x\ \upsilon \rfloor$$

The nonzero elements of the coefficient matrix are

$A(1,4) = -\varepsilon/2$; $A(1,5) = -\xi/2$; $A(1,12) = -1/EA$;

$A(2,4) = 1$; $A(3,5) = 1$; $A(4,4) = -a_1M_x$;

$A(4,5) = a_3M_x$; $A(4,6) = (-a_4M_z - 2a_1M_y)$; $A(4,8) = a_1$;

$A(4,9) = -a_3$; $A(5,4) = -a_2M_x$; $A(5,5) = a_1M_x$;

$A(5,6) = (-2a_1M_z + a_4M_y)$; $A(5,8) = a_2$; $A(5,9) = -a_1$;

$A(6,4) = M_z/GJ$; $A(6,5) = M_y/GJ$; $A(6,7) = 1/GJ$;

$A(7,3) = m\Omega^2 e \sin\theta$; $A(7,4) = (V_y + k_3k_4\Omega^2 x v$

$- k_3k_1k_4\Omega^2 x - k_4c^2\Omega^2 x/16)$;

$$A(7,5) = -V_z;\ A(7,6) = m\Omega^2(k_{m_2}^2 - k_{m_2}^2)(\cos 2\theta - \phi\cos\theta\sin\theta)$$
$$+ \Omega^2 e\cos\theta v\ - k_3k_4\Omega^2x^2;$$
$$A(7,13) = k_3k_4\Omega^2x^2;\ A(8,5) = V_x;\ A(8,6) = -m\Omega^2 e x\sin\theta;$$
$$A(8,10) = -1;\ A(9,4) = -V_x;\ A(9,6) = -m\Omega^2 e x\cos\theta;$$
$$A(9,11) = 1;\ A(10,3) = -m\Omega^2;\ A(10,4) = k_4\Omega v_i k_1;$$
$$A(10,6) = m\Omega^2 e\sin\theta + k_4\Omega x v_i;\ A(11,4) = -k_4(k_1 - v)\Omega^2 x;$$
$$A(11,6) = -k_4\Omega^2x^2;\ A(11,13) = -k_4\Omega^2x^2;\ A(13,5) = (M_z a_1 - M_y a_3)$$

where $k_1 = c(1-e)/2$ $\qquad$ $k_3 = ce/2$

$k_2 = c_d/a$ $\qquad$ $k_4 = \rho ac/2$

The nonzero elements of the nonhomogeneous excitation vector are

$$f(7) = \Omega^2 m(k_{m_2}^2 - k_{m_1}^2)\cos\theta\sin\theta + k_3k_4\Omega x v_i - k_3k_4\Omega^2x^2\theta$$
$$- k_3k_4\Omega^2 x k_1\beta_{pc} + k_4\frac{c^2}{16}\beta_{pc}$$
$$f(8) = \Omega^2 e x\cos\theta$$
$$f(9) = -m\Omega^2 e x\sin\theta$$
$$f(10) = -m\Omega^2 e\cos\theta + k_4\{-v_i + \Omega^2x^2k_2 + \Omega x v_i\theta + k_1\Omega v_i\beta_{pc}\}$$
$$f(11) = k_4\Omega x v_i - k_4\Omega^2x^2\theta + m\Omega^2 x\beta_{pc} - k_4\Omega^2 x k_1\beta_{pc}$$
$$f(12) = -m\Omega^2 x$$

4.2 Iteration Scheme for Nonlinear Differential Equations

The overall scheme is to first solve a standard, linear problem and then use these results to simplify and solve the more complicated nonlinear problem.

The following two equations are linearized forms of the nonlinear equation (4.1). Both satisfy all the appropriate boundary conditions.

$$\{z^{(1)}(x)\}' = [A(x,z)_{z=0}]\ \{z^{(1)}(x)\} + \{f\} \qquad (4.1a)$$

$$\{z^{(2)}(x)\}' = [A(x,z)_{z=z^{(1)}}]\ \{z^{(2)}(x)\} + \{f\} \qquad (4.1b)$$

The two solutions denoted by $\{z^{(1)}(x)\}$ and $\{z^{(2)}(x)\}$ are defined as the first and second approximate solutions of equation (4.1).

Equation (4.1a) is simply equation (4.1) linearized by the starting assumption $\{z(x)\} = \{0\}$ in the coefficient matrix [A]. Its solution $\{z^{(1)}(x)\}$ = is a linear solution to equation (4.1).

The solution $\{z^{(1)}(x)\}$ is then used to linearize the coefficient matrix $[A(x,z)_{z=z^{(1)}}]$ in equation (4.1b). Solution of equation (4.1b) yields $\{z^{(2)}(x)\}$, and $\{z^{(2)}(x)\}$represents the first nonlinear solution to equation (4.1). The second nonlinear solution is based on

$$\{z^{(3)}(x)\} = \{z^{(2)}(x)\} + \{\Delta z^{(2)}(x)\} \qquad (4.2)$$

where $\{\Delta z^{(2)}(x)\}$ is an incremental solution. To a first order, the incremental solution is governed by the following equation.

$$\{\Delta z^{(2)}(x)\}' = ([A(x,z^{(2)})] + [B(x,z^{(2)})])\ \{\Delta z^{(2)}(x)\} - \{y_u^{(2)}(x)\} \qquad (4.3)$$

where $\{y_u^{(2)}(x)\}$ is the unbalanced load and is given by

$$\{y_u^{(2)}\} = \{z^{(2)}(x)\}' - [A(x,z^{(2)})]\ \{z^{(2)}(x)\} - \{f\}$$

Equation (4.1b) can be used to rewrite the above equation for the unbalanced load as

$$\{y_u^{(2)}(x)\} = ([A(x,z^{(1)})] - [A(x,z^{(2)})])\ \{z^{(2)}(x)\} \tag{4.4}$$

The j^{th} column of matrix $[B(x,z^{(2)})]$ denoted by $\{B_j\}$ is given by

$$\{B_j\} = \left(\frac{\partial}{\partial z_j}[A(x,z)]\right)_{z=z^{(2)}} \{z^{(2)}\} \tag{4.5}$$

where z_j is the j^{th} element of the state vector $\{z\}$. Since $\{z^{(3)}(x)\}$ and $\{z^{(2)}(x)\}$ satisfy the same set of boundary conditions, the incremental solution vector $\{\Delta z^{(2)}(x)\}$ satisfies the following zero boundary conditions by virtue of equation (4.2).

$$\{\Delta z^{(2)}(x)\} = \{0\} \text{ at boundary points} \tag{4.6}$$

Now the incremental solution is obtained by solving equations (4.3) through (4.6). Once $\{\Delta z^{(2)}(x)\}$ is known the third approximate solution $\{z^{(3)}(x)\}$ is given by equation (4.2). In general, for the i^{th} iterate equations (4.2) through (4.6) may be written as

$$\{z^{(i+1)}(x)\} = \{z^{(i)}(x)\} + \{\Delta z^{(i)}(x)\} \tag{4.7a}$$

where

$$\{\Delta z^{(i)}(x)\}' = ([A(x,z^{(i)})] + [B(x,z^{(i)})])\ \{\Delta z^{(i)}(x)\} - \{y_u^{(i)}(x)\} \tag{4.7b}$$

and

$$\{y_u^{(i)}(x)\} = ([A(x,z^{(i-1)})] - [A(x,z^{i})])\ \{z^{(i)}(x)\} \tag{4.7c}$$

and

$$\{B_j\} = \left(\frac{\partial}{\partial z_j}[A(x,z^{(i)})\right)\{z^{(i)}(x)\} \tag{4.7d}$$

$$\{\Delta z^{(i)}(x)\} = \{0\} \text{ at boundary points} \tag{4.7e}$$

A few iterations of equations (4.7) are required to achieve convergence for the nonlinear steady deflections. This procedure is essentially equivalent to the quasi-linearization method of solving nonlinear boundary value problems [42].

4.3 Static Transfer Matrix and Solution

The starting and the subsequent iteration solutions (equations (4.2) - (4.7) involve the solution of a linearized branched boundary value problem of the following form.

$$\{z(x)\}' = [A(x)]\ \{z(x)\} + \{f\} \tag{4.8}$$

The transfer matrix for the homogeneous part of this equation is static (time independent) and is given by [23] as

$$[T(x)]' = [A(x)]\ [T(x)] \tag{4.9}$$

with the initial conditions

$$[T(0)] = [I] \tag{4.10}$$

The static transfer matrix is used to construct the homogeneous solution. Taken together with the particular integral the complete nonhomogeneous solution for equation (4.8) can be written as in reference [26]

$$\{z(x)\} = [T(x,0)]\,\{z(0)\} + [T(x,0)] \int_0^x [T(s,0)]^{-1}\,\{f(s)\}ds \qquad (4.11)$$

4.4 Formulation

From equation (4.11), the following relation can be written between the state vectors at locations 2 and 3 on the blade (see Figure 3.1)

$$\{z_3\} = [T]\,\{z_2\} + \{c\} \qquad (4.12)$$

This equation may be rewritten in an expanded form relating deflections (d) and forces (f).

$$\begin{Bmatrix} d_3 \\ - - - \\ f_3 \end{Bmatrix} = \left[\begin{array}{c|c} T_{11} & T_{12} \\ - - - - & - - - - \\ T_{21} & T_{22} \end{array}\right] \begin{Bmatrix} d_2 \\ - - - \\ f_2 \end{Bmatrix} + \begin{Bmatrix} c_1 \\ - - - \\ c_2 \end{Bmatrix} \qquad (4.13)$$

Similarly, the transfer matrix relation for the i^{th} load path can be written (see Figure 3.1)

$$\{z_2^i\} = [T^i]\,\{z_1^i\} + \{c^i\} \qquad (4.14)$$

Expanding the above equation into a partitioned form gives

$$\left\{\begin{array}{c} d_2^i \\ - - - \\ f_3^i \end{array}\right\} = \left[\begin{array}{c|c} T_{11}^i & T_{12}^i \\ - - - - & - - - - \\ T_{21}^i & T_{22}^i \end{array}\right] \left\{\begin{array}{c} d_1^i \\ - - - \\ f_1^i \end{array}\right\} + \left\{\begin{array}{c} c_1^i \\ - - - \\ c_2^i \end{array}\right\} \quad (4.15)$$

The transfer matrices in the above equations are determined from equations (4.9) and (4.10) and the nonhomogeneous solution vector {c} is obtained from equation (4.11).

In general, boundary conditions are defined at the branch roots and the blade tip. Equilibrium (equation (3.2)) and compatibility (equation (3.4)) relate the state vector between the blade root and the branch tips (across the clevis).

The boundary condition at the blade tip is

$$\{f_3\} = \{0\} \quad (4.16)$$

The root ends of the branches are assumed either as clamped in bending and extension and either clamped or spring restrained in torsion. However, the formulation allows for different root conditions. The number of branches is also kept general:

$$\text{clamped:} \quad \{d_1^i\} = \{0\} \quad (4.17)$$

spring restrained (torsion):

$$\left.\begin{array}{l} u_1 = v_1 = w_1 = 0;\ \phi_1 = M_{x_1}/k\phi \\ M_{y_1} = 0,\ \ M_{z_1} = 0 \end{array}\right\} \quad (4.18)$$

where k_ϕ = control system stiffness.

From equation (4.15)

$$\{d_2^i\} = [T_{11}^i]\ \{d_1^i\} + [T_{12}^i]\ \{f_1^i\} + \{c_1^i\} \tag{4.19}$$

$$\{f_2^i\} = [T_{21}^i]\ \{d_1^i\} + [T_{22}^i]\ \{f_1^i\} + \{c_2^i\} \tag{4.20}$$

From Eq. (4.19)

$$\{f_1^i\} = [T_{12}^i]^{-1}\{d_2^i\} - [T_{12}^i]^{-1}\{T_{11}^i\}\{d_1^i\} - [T_{12}^i]^{-1}\ \{c_1^i\} \tag{4.21}$$

Apply compatibility across the clevis. Substitute equation (3.4) into (4.21)

$$\{f_1^i\} = [T_{12}^i]^{-1}[B^i]^{-1}\{d_2\} - [T_{12}^i]^{-1}[T_{11}^i]\{d_1^i\} - [T_{12}^i]([B^i]^{-1}\{b\} + \{c_1^i\}) \tag{4.22}$$

Eq. (4.22) for clamped branches can be written by applying the root boundary condition (4.17)

$$\{f_1^i\} = [r^i]\ \{d_2\} + \{e^i\} \tag{4.23}$$

where

$$[r^i] = [T_{12}^i]^{-1}[B^i]^{-1} \tag{4.24}$$

$$\{e_1^i\} = -[T_{12}^i]^{-1}([B^i]^{-1}\{b\} + \{c_1^i\}) \tag{4.25}$$

For spring restrained branches, equation (4.22) remains as

$$\{f_1^i\} = [r^i]\ \{d_2\} + [s^i]\ \{d_1^i\} + \{e^i\} \tag{4.26}$$

Expanding Eq. (4.26) and substituting boundary conditions given by Eq. (4.18) yields

$$\begin{Bmatrix} M_{x1}^1 = k_\phi \phi_1^i \\ 0 \\ 0 \\ \hline V_{y1}^i \\ V_{z1}^i \\ V_{x1}^i \end{Bmatrix} = \left[\begin{array}{c|c} r_{11} & r_{12} \\ \hline r_{21} & r_{22} \end{array}\right] \begin{Bmatrix} l_{d_2} \\ \hline r_{d_2} \end{Bmatrix}$$

$$+ \left[\begin{array}{c|c} s_{11} & s_{12} \\ \hline s_{21} & s_{22} \end{array}\right] \begin{Bmatrix} 0 \\ \hline \varepsilon_1^i \\ \xi_1^i \\ \phi_1^i \end{Bmatrix} + \begin{Bmatrix} e_1^i \\ \hline e_2^i \end{Bmatrix} \qquad (4.27)$$

Extract the top three equations of Eq. (4.27) and rewrite as

$$\begin{bmatrix} 0 & 0 & k_\phi \\ 0 & 0 & 0 \\ 0 & 0 & 0 \end{bmatrix} \begin{Bmatrix} \varepsilon_1^i \\ \xi_1^i \\ \phi_1^i \end{Bmatrix} = [r_{11}] \{l_{d_2}\} + [r_{12}] \{r_{d_2}\}$$

$$+ [s_{12}] \begin{Bmatrix} \varepsilon_1^i \\ \xi_1^i \\ \phi_1^i \end{Bmatrix} + \{e_1^i\} \tag{4.28}$$

Rewriting Eq. (4.28),

$$[p] \begin{Bmatrix} \varepsilon_1^i \\ \xi_1^i \\ \phi_1^i \end{Bmatrix} = [r_{11}] \{l_{d_2}\} + [r_{12}] \{r_{d_2}\} + \{e_1^i\} \tag{4.29}$$

where $$[p] = \begin{bmatrix} 0 & 0 & k_\phi \\ 0 & 0 & 0 \\ 0 & 0 & 0 \end{bmatrix} - [s_{12}]$$

From Eqs. (4.29) and (4.18)

$$\{d_1^i\} = [a^i] \{d_2\} + \{m^i\} \tag{4..30}$$

where

$$[a^i] = \left[\begin{array}{c|c} [0] & [0] \\ \hline [p]^{-1}[r_{11}] & [p]^{-1}[r_{21}] \end{array}\right] \tag{4.31}$$

$$\{m^i\} = \begin{bmatrix} 0 \\ \hline [p]^{-1}\{e_1^i\} \end{bmatrix} \tag{4.32}$$

Substituting Eq. (4.30) into Eq. (4.26) yields

$$\{f_1^i\} = ([r^i] + [s^i]\,[a^i])\,\{d_2\} + [s^i]\,\{m^i\} + \{e^i\} \tag{4.33}$$

For clamped branches, the boundary condition (4.17) can be applied to equation (4.20)

$$\{f_2^i\} = [T^i_{22}]\ \{f_1^i\} + \{c_2^i\} \tag{4.34}$$

Substituting Eq. (4.23) into Eq. (4.34) gives

$$\{f_2^i\} = [k^i]\,\{d_2\} + \{l^i\} \tag{4.35}$$

where

$$[k^i] = [T^i_{22}]\ [r^i] \tag{4.36}$$

$$[l^i] = [T^i_{22}]\ \{e^i\} + \{c_2^i\} \tag{4.37}$$

For spring restrained branches, substituting Eq. (4.30) into Eq. (4.20) gives

$$\{f_2^i\} = [k^i]\,\{d_2\} + \{l^i\} \tag{4.38}$$

$$[k^i] = [T^i_{22}]\ [r^i] + ([T^i_{21}] + [T^i_{22}]\ [s^i]) + [a^i] \tag{4.39}$$

$$[l^i] = [T^i_{22}]\ \{e^i\} + [c_2^i] + ([T^i_{21}] + [T^i_{22}]\ [s^i])\ \{m^i\} \tag{4.40}$$

Substituting Eq. (4.35) or Eq. (4.38) into the equilibrium equation (3.2) across the clevis yields

$$[f_2] = [k_1]\,\{d_2\} + \{k_2\} \tag{4.41}$$

where

$$[k_1] = \sum_{i=1}^{n} [A^i]\ [k^i] \tag{4.42}$$

$$[k_2] = \sum_{i=1}^{n} [A^i]\ \{l^i\} \tag{4.43}$$

From Eq. (4.13)

$$\{f_3\} = [T_{21}]\ \{d_2\} + [T_{22}]\ \{f_2\} + \{c_2\} \tag{4.44}$$

Substituting Eq. (4.41) into Eq. (4.44) yields

$$\{f_3\} = ([T_{21}] + [T_{22}]\ [k_1])\ \{d_2\} + [T_{22}]\ \{k_2\} + \{c_2\} \tag{4.45}$$

From applying the boundary condition for the blade (Eqs. (4.16) - (4.45))

$$\{d_2\} = -([T_{21}] + [T_{22}]\ [k_1])^{-1}\ ([T_{22}]\ \{k_2\} + \{c_2\}) \tag{4.46}$$

Now the state vector $\{z_2\}$ is known from Eqs. (4.46) and (4.41). The state vector $\{z_1^i\}$ for the spring restrained branches can be obtained from Eqs. (4.30) and (4.33). For clamped branches $\{d_1^i\} = \{0\}$ by virtue of the boundary condition and $\{f_1^i\}$ can be computed from Eq. (4.23). Once the state vectors $\{z_1^i\}$ and $\{z_2\}$ are known, the solutions at any station can be determined from Eq. (4.11) as shown below.

i^{th} branch:

$$\{z^i(x)\} = [T^i(x)]\ \{z_1^i\} + \{c^i\} \tag{4.47}$$

blade:

$$\{z(x)\} = [T(x)]\ \{z_2\} + \{c\} \tag{4.48}$$

For blades with single root branches, the boundary conditions are assumed as shown below.

$$x = 0:\ u = w = v = \varepsilon = \xi = 0 \qquad \phi = \frac{M_x}{k_\phi} \tag{4.49}$$

$$x = R:\ \{f_3\} = \{0\} \tag{4.50}$$

The equilibrium and compatibility matrices become identity matrices and this yields

$$\{d_2\} = \{d_2^1\} = [T^{\,1}_{1\,1}]\ \{d_1\} + [T^{\,1}_{1\,2}]\ \{f_1\} + \{c_1\} \tag{4.51}$$

$$\{f_2\} = \{f_2^1\} = [T^{\,1}_{2\,1}]\ \{d_1\} + [T^{\,1}_{2\,2}]\ \{f_1\} + \{c_2\} \tag{4.52}$$

Substitute Eqs. (4.50) to (4.52) into Eq. (4.45) yields

$$[A]\ \{d_1\} + [B]\ \{f_1\} + \{E\} = \{0\} \tag{4.53}$$

where

$$[A] = [T_{21}]\ [T^{\,1}_{1\,1}] + [T_{22}]\ [T^{\,1}_{2\,2}\ ]$$
$$[B] = [T_{21}]\ [T^{\,1}_{1\,2}] + [T_{22}]\ [T^{\,1}_{2\,2}\ ]$$
$$[C] = [T_{21}]\ [c_1^1]\ + [T_{22}]\ [c_2^1]$$

Substituting Eq. (4.49) into Eq. (4.53) yields the following equation for ϕ_1.

$$\phi_1 = -\lfloor a\ 0\ 0\ 0\ 0\ 0 \rfloor [B]^{-1}\{E\} \tag{4.54}$$

where

$$a = 1/(D_{1,6} + k_\phi)$$

and

$$[D] = [B]^{-1}\,[A]$$

Once ϕ_1 is known, $\{d_1\}$ is known and $\{f_1\}$ can be computed from Eq. (4.53) as shown below.

$$\{f_1\} = -[B]^{-1}[A]\,\{d_1\} - [B]^{-1}[E] \tag{4.55}$$

Once the state vector $\{z_1\}$ is known, the solution at any station can be computed from the following equations.

branch:

$$\{z(x)\} = [T^1(x)]\,\{z_1\} + \{c\} \tag{4.56}$$

blade:

$$\{z(x)\} = [T(x)]\,\{z_2\} + \{c\} \tag{4.57}$$

4.5 Solution Procedure

As described in section 4.2, the linear solution is taken as the starting solution for the iterations. The linear solution is obtained by

solving Eq. (4.1) with $\{z(x)\} = \{0\}$ in the coefficient matrix except for the tension V_x. The tension in the blade is obtained as shown below.

$$V_x(x) = \int_x^R \Omega^2 m x \, dx \tag{4.58}$$

The tensions in the branches are calculated by assuming that the branches are coincident with the blade at the clevis, i.e., $h_y^i = h_y^i = 0$. The tensions corresponding to this case are calculated as follows. The transfer matrix for axial motion of a beam for the static case is given by

$$[T(x)] = \begin{bmatrix} 1 & a \\ 0 & 1 \end{bmatrix} \tag{4.59}$$

where $$a = \int_o^x \frac{1}{EA} \, dx$$

By definition of the transfer matrix

$$\begin{Bmatrix} u_2^i \\ V_{x2}^i \end{Bmatrix} = \begin{bmatrix} 1 & a_i \\ 0 & 1 \end{bmatrix} \begin{Bmatrix} u_1^i = 0 \\ V_{x1}^i \end{Bmatrix} \tag{4.60}$$

From the above equation

$$\left.\begin{aligned} u_2^i &= a_i V_{x1}^i \\ V_{x2}^i &= V_{x1}^i \end{aligned}\right\} \tag{4.61}$$

The following two cases are considered

Case 1: 2 branches

Expansion of Eq. (4.61) yields

$$\left.\begin{aligned} u_2^1 &= a_1 V_{x2}^1 \\ u_2^2 &= a_2 V_{x2}^2 \end{aligned}\right\} \tag{4.62}$$

For coincident nodes ($u_2^1 = u_2^2$), Eq. (4.62) becomes

$$a_1 V_{x2}^1 - a_1 V_{x2}^2 = 0 \tag{4.63}$$

For equilibrium

$$V_{x2}^1 + V_{x2}^2 = V_{x2} \tag{4.64}$$

Solving Eqs. (4.63) and (4.64) gives

$$\left.\begin{aligned} V_{x2}^1 &= \frac{a_2}{a_1 + a_2} V_{x2} \\ V_{x2}^2 &= \frac{a_1}{a_1 + a_2} V_{x2} \end{aligned}\right\} \tag{4.65}$$

Case 2: 3 branches

Expanding Eq. (4.61) for coincident nodes yields

$$a_1 V_{x2}^1 = a_2 V_{x2}^2 = a_3 V_{x2}^3 \tag{4.66}$$

For equilibrium

$$V^1_{x2} + V^2_{x2} + V^3_{x3} = V_{x2} \tag{4.67}$$

By solving Eqs. (4.66) and (4.67) yields

$$\left.\begin{aligned} V^1_{x2} &= a_2 a_3 V_{x2}/D \\ V^2_{x2} &= a_3 a_1 V_{x2}/D \\ V^3_{x2} &= a_1 a_2 V_{x2}/D \end{aligned}\right\} \tag{4.68}$$

where $D = a_1a_2 + a_2a_3 + a_3a_1$

Now the above result can be generalized to the 'n' branch case as shown below.

$$V^i_{x2} = \frac{\sum_{j=1}^{n,i} a_j}{\sum_{k=1}^{n} \left(\sum_{j=1}^{n,k} a_j\right)} \tag{4.69}$$

where $\sum_{j=1}^{n,i} = a_1 a_2 \ldots a_n/a_i$

and V_{x2} is obtained from Eq. (4.58).

Now the tension in the ith branch corresponding to the coincident branch case is given by

$$V^i_x(x) = \int_x^l \Omega^2 m x dx + V^i_{x2} \tag{4.70}$$

Once V_x in the branches and the blade is known, the linear steady state solution can be obtained following the procedure outlined in Section 4.4. Note that for the single branch case, the V_x is simply given by equation (4.58) in both the branch and blade.

5. LINEAR PERTURBATION EQUATIONS

In the absence of experimental flight testing, the aeroelastic characteristics of any flight vehicle in trimmed flight may be investigated using perturbation equations. The procedure for the development of perturbation equations is universal for all flight dynamics problems. Here the complete perturbation equations for an investigation of the flight dynamic instabilities of an isolated rotor blade are presented. Components of such an aeroelastic analysis are i) free vibration characteristics about the nonlinearly deformed steady state and iii) complex stability eigenvalues. In the present work, the equations below are utilized to investigate each of these three elements.

The procedure for the development of the linear perturbation equations is

1. Substitute $\{z(\bar{x},t)\} = \{z_0(x)\} + \{z^p(x,t)\}$ into the governing differential equations (2.7), (2.8), (2.9) and (2.33-2.41) and 2.80-2.82.
2. Subtract the nonlinear steady state equations (4.1) from the results of step 1. This step will eliminate all steady state and nonhomogeneous terms.
3. Drop the nonlinear terms in the perturbed variables $\{z^p(x,t)\}$.

The resulting linearized homogeneous perturbation equations are listed below (with the bars omitted for simplicity).

$$u' = -\varepsilon_o\varepsilon - \xi_o\xi + V_x/EA \tag{5.1}$$

$$w' = \varepsilon \tag{5.2}$$

$$v' = \xi \tag{5.3}$$

$$\begin{aligned}\varepsilon' = {} & -a_1 M_{x_o}\varepsilon + a_3 M_{x_o}\xi - (2a_1 M_{y_o} + a_4 M_{z_o})\phi \\ & + (-a_1\varepsilon_o + a_1\xi_o)M_X + (a_1 - a_4\phi_o)M_Z \\ & - (a_3 + 2a_1\phi_o)M_y\end{aligned} \tag{5.4}$$

$$\begin{aligned}\xi' = {} & -a_2 M_{x_o}\varepsilon + a_1 M_{x_o}\xi - (2a_1 M_{z_o} - a_4 M_{y_o})\phi \\ & + (-a_2\varepsilon_o + a_1\xi_o)M_x \\ & + (a_2 - 2a_1\phi_o)M_z - (a_1 - a_4\phi_o)M_y\end{aligned} \tag{5.5}$$

$$\phi' = (1/GJ)\,(M_{z_o}\varepsilon + M_{y_o}\xi + M_x + \varepsilon_o M_z + \xi_o M_y) \tag{5.6}$$

$$\begin{aligned}M_x' = {} & -2me\Omega\sin\theta\dot{u} + me(\cos\theta - \phi_o\sin\theta(\ddot{w} \\ & - me(\sin + \phi_o\cos\theta(\ddot{v} - \Omega^2 v) \\ & + 2\Omega m(k_{m_2}^2\sin\theta + k_{m_1}^2\cos^2\theta\dot{\varepsilon} + V_{y_o}\varepsilon \\ & + 2\Omega m(k_{m_2}^2 - k_{m_1}^2)\cos\theta\sin\theta\dot{\xi} - V_{z_o}\xi + mk_m^2\ddot{\phi} \\ & + \Omega^2 m(k_{m_2}^2 - k_{m_1}^2)\cos^2\theta - \phi_o\sin^2\theta) + me\Omega^2 v_o\cos\theta\}\phi \\ & + \varepsilon_o V_y - \xi_o V_z - M_e\end{aligned} \tag{5.7}$$

$$M_z' = 2me\Omega\cos\theta\dot{v} + V_{x_o}\xi - me\Omega^2 x\sin\theta\phi - V_y + \xi_o V_x \tag{5.8}$$

$$M_y' = 2me\Omega\sin\theta\dot{v} - V_{x_o}\varepsilon - me\Omega^2 x\cos\theta\phi + V_z - \varepsilon_o V_x \qquad (5.9)$$

$$V_y' = 2\Omega m\dot{u} + m(\ddot{v}-\Omega^2 v) - 2\Omega me\sin\theta\dot{\varepsilon} - 2\Omega me\cos\theta\dot{\xi} + me\sin\theta(\Omega^2\phi-\ddot{\phi}) - L_v - 2\Omega m\beta_{pc}\dot{w} \qquad (5.10)$$

$$V_z' = m\ddot{w} + me\cos\theta\ddot{\phi} - L_w + 2m\Omega\beta_{pc}\dot{v} \qquad (5.11)$$

$$V_x' = m(\ddot{u}-\Omega^2 u) - 2\Omega m\dot{v} \qquad (5.12)$$

where the perturbed aerodynamic forcing functions are

$$L_v = k_4[-\Omega x v_{i_o}\phi - \{2\Omega x k_2 + (\theta+\phi_o)v_{i_o}\}\dot{v} + \{2v_{i_o} - \Omega x(\theta+\phi_o)_{i_o}\}\dot{w} - k_1 v_{i_o}(\phi+\Omega\varepsilon) - \Omega k_1(\varepsilon_o+\beta_{pc})_{i_o}\}\dot{w}] \qquad (5.13)$$

$$L_w = k_4[\Omega^2 x^2\phi - \Omega^2 x(v_o\varepsilon+\varepsilon_o v) - \Omega^2 x\beta_{pc})v + k_1\Omega^2 x\varepsilon + \{2\Omega x(\theta+\phi_o) - v_{i_o} + \Omega k_1(\varepsilon_o+\beta_{pc})\}\dot{v} - \Omega x\dot{w} + k_1\Omega x\dot{\phi}) \qquad (5.14)$$

$$M_e = k_3 L_w - k_4 c^2[\Omega x\ \}\dot{\phi} + \Omega^2 x\varepsilon + \Omega(\varepsilon_o+\beta_{pc}))\}\dot{v} \qquad (5.15)$$

and

$k_1 = c(1-e)/2$ $\qquad$ $k_3 = ce/2$

$k_2 = c_d/a$ $\qquad$ $k_4 = \rho ac/2$

6. FREE VIBRATION CHARACTERISTICS

6.1 Equations for Free Vibration

The free vibration equations are a special case of the complete linear perturbation equations developed in Chapter 5 (equations (5.1) - (5.12)). The free vibration equations are developed from the linear perturbation equations by the following procedure.

1. Drop damping type terms, i.e. terms containing first derivatives with respect to time ($\dot{u}, \dot{v}, \dot{w}, \dot{\varepsilon}, \dot{\xi}, \dot{\phi}$)
2. Eliminate time dependency in the equations by assuming simple harmonic motion with frequency ω for u, w, v and ϕ.

$$\{z(x,t)\} = Ze^{i\omega t}$$

3. Drop all the aerodynamic loadings (forcing functions).

The resulting equations are summarized below:

$$u' = -\varepsilon_o\varepsilon - \xi_o\xi + V_x/EA \tag{6.1}$$

$$w' = \varepsilon \tag{6.2}$$

$$v' = \xi \tag{6.3}$$

$$\varepsilon' = a_1 M_{x_o}\varepsilon + a_3 M_{x_o}\xi - (2a_1 M_{y_o} + a_4 M_{z_o})\phi + (-a_1\varepsilon_o + a_3\xi_o)M_x + (a_1 - a_4\phi_o)M_z - (a_3 + 2a_1\phi_o)M_y \tag{6.4}$$

$$\xi' = -a_2 M_{x_o}\varepsilon + a_1 M_{x_o}\xi + (a_4 M_{y_o} - 2a_1 M_{z_o})\phi + (a_1\xi_o - a_2\varepsilon_o)M_x + (a_2 - 2a_1\phi_o)M_z + (-a_1 + a_4\phi_o)M_y \tag{6.5}$$

$$\phi' = (1/GJ)(M_{z_o}\varepsilon + M_{y_o}\xi + M_x + \varepsilon_o M_z + \varepsilon_o M_y) \tag{6.6}$$

$$M_x' = -\omega^2 me\Omega(\cos\theta - \phi_o \sin\theta)w + me(\sin\theta + \phi_o \cos\theta)(\omega^2 + \Omega^2)v + V_{y_o}\varepsilon - V_{z_o}\xi + \{-\omega^2 k_m^2 + \Omega^2 m(k_{m_2}^2 - k_{m_1}^2)(\cos 2\theta - \phi_o \sin 2\theta) + me\Omega^2 v_o \cos\theta\}\phi + \varepsilon_o v_y - \xi_o v_z \tag{6.7}$$

$$M_z' = V_{x_o}\xi - me\Omega^2 x \sin\theta\phi - V_y + \xi_o V_x \tag{6.8}$$

$$M_y' = -V_{x_o}\varepsilon - me\Omega^2 x \cos\theta\phi + V_z - \varepsilon_o V_x \tag{6.9}$$

$$V_y' = -(\omega^2 + \Omega^2)mv + (\omega^2 + \Omega^2)me\sin\theta\phi \tag{6.10}$$

$$V_z' = -\omega^2 mw - me\omega^2 \cos\theta\phi \tag{6.11}$$

$$V_x' = -(\omega^2 + \Omega^2)mu \tag{6.12}$$

Equations (6.1) to (6.12) govern the free-vibration state about the nonlinear steady state position. Equations of motion governing the

free-vibration state about the initial geometry can be obtained by substituting the following relations in the above equations.

$$u_o = v_o = w_o = \varepsilon_o = \xi_o = \phi_o = M_{x_o} = M_{y_o} = M_{z_o} = 0 \qquad (6.13)$$

$$\left.\begin{aligned} V_{x_o} &= \int_x^R \Omega^2 m x \, dx \\ V_{y_o} &= \Omega^2 m x e \cos\phi \\ V_{z_o} &= \Omega m x e \sin\beta \end{aligned}\right\} \qquad (6.14)$$

6.2 Dynamic Transfer Matrix

The first-order differential equations of motion are linear and homogeneous and therefore can be arranged into a matrix differential equation of the following form:

$$\{z(x)\}' = [A(x)]\,[T(x)] \qquad (6.15)$$

The transfer matrix for the above system is given by solving the following equations.

$$[T(x)]' = [A(x)]\,[T(x)] \qquad (6.16)$$

$$[T(0)] = [I] \qquad (6.17)$$

Once the transfer matrix is known the free-vibration characteristics of branched blades can be determined in the following section.

6.3 Frequency Determinant

To compute the natural frequencies of the branched blade, a frequency determinant is computed and scanned for different input frequencies until the value of the determinant is zero. The input frequency that returns a zero value for the frequency determinant is a natural frequency of the system. Since the branches and blade are modeled separately, the frequency determinant is constructed by relating the state vectors at the branch roots to the state vector at the blade tip.

By definition of the transfer matrix, the following relation between state vectors at locations 2 and 3 can be written (see Figure 3.1)

$$\{z_3\} = [T]\,\{z_2\} \tag{6.18}$$

Rewriting this equation into the following partitioned form:

$$\begin{Bmatrix} d_3 \\ - - - \\ f_3 \end{Bmatrix} = \left[\begin{array}{c|c} T_{11} & T_{12} \\ - - - & - - - \\ T_{21} & T_{22} \end{array}\right] \begin{Bmatrix} d_2 \\ - - - \\ f_2 \end{Bmatrix} \tag{6.19}$$

Extracting the following equation for forces from Eq. (6.18) yields

$$\{f_3\} = [T_{21}]\,\{d_2\} + [T_{22}]\,\{f_2\} \tag{6.20}$$

Similarly, the transfer matrix relation for the ith branch can be written as (see Figure 3.1)

$$\{z_2^i\} = [T^i]\ \{z_1^i\} \tag{6.21}$$

Rewriting the above equation into partitioned form:

$$\begin{Bmatrix} d_2^i \\ - - - \\ f_2^i \end{Bmatrix} = \left[\begin{array}{c|c} T_{11}^i & T_{12}^i \\ - - - & - - - \\ T_{21}^i & T_{22}^i \end{array}\right] \begin{Bmatrix} d_1^i \\ - - - \\ f_1^i \end{Bmatrix} \tag{6.22}$$

Expanding Eq. (6.22) gives

$$\{d_2^i\} = [T_{11}^i]\ \{d_1^i\} + [T_{12}^i]\ \{f_1^i\} \tag{6.23}$$

$$\{f_2^i\} = [T_{21}^i]\ \{d_1^i\} + [T_{22}^i]\ \{f_1^i\} \tag{6.24}$$

The boundary conditions for the branch roots are given by

Clamped: $\{d_1\} = 0$ (6.25)

Spring Restrained: $u_1 = v_1 = w_1 = M_{y_1} = M_{z_1} = 0$ (6.26)

For homogeneous problems, the collective pitch can be added to the pretwist of the blade and this will translate as elastic twist to the branches. For free-vibration problems, the steady state elastic twists of the branches have to be determined to solve the homogeneous problem. Once this is done, the compatibility relation given by Eq. (3.4) can be written as

$$\{d_2\} = [B^i]\ \{d_2^i\} \tag{6.27}$$

If the free-vibration is solved about the undeformed state, the elastic twist of the branches due to collective pitch should be included as pretwist of the branches. The equilibrium equation across the clevis will be same as before as given by Eq. (3.4).

$$\{f_2\} = \sum_{i=1}^{n} [A^i] \{f_2^i\}$$

Two cases are considered here (clamped and spring restrained branches).

1. Clamped branches

   By virtue of the boundary condition equation (6.25), equations (6.23) and (6.24) become

$$\{d_2^i\} = [T_{12}^i] \{f_1^i\} \tag{6.28}$$

$$\{f_2^i\} = [T_{22}^i] \{f_1^i\} \tag{6.29}$$

From Eq. (6.28)

$$\{f_1^i\} = [T_{12}^i]^{-1} \{d_2^i\} \tag{6.30}$$

Substituting the compatibility Eq. (6.27) into Eq. (6.30) gives

$$\{f_1^i\} = [T_{12}^i]^{-1} [B^i]^{-1} \{d_2\} \tag{6.31}$$

Substituting Eq. (6.31) into Eq. (6.29) yields an expression for forces in the clamped branches at the clevis

$$\{f_2^i\} = [T_{22}^i]\ [T_{12}^i]^{-1}\ [B]^{-1}\ \{d_2\} \tag{6.32}$$

or $\{f_2^i\} = [k^i]\ \{d_2\}$

where $$[k^i] = [T_{22}^i]\ [r^i] \tag{6.33}$$

$$[r^i] = [T_{12}^i]^{-1}\ [B^i]^{-1} \tag{6.34}$$

2. Spring restrained branches

From Eq. (6.23)

$$\{f_1^i\} = [T_{12}^i]^{-1}\{d_2^i\} - [T_{12}^i]^{-1}\ [T_{11}^i]\ \{d_1^i\} \tag{6.35}$$

Substituting the compatibility Eq. (6.27) into Eq. (6.35) gives

$$\{f_1^i\} = [T_{12}^i]^{-1}\ [B^i]^{-1}\ \{d_2\} - [T_{12}^i]^{-1}\ [T_{11}^i]\ \{d_1^i\} \tag{6.36}$$

Rewriting Eq. (6.36) as

$$\{f_1^i\} = [r^i]\ \{d_2\} + [s^i]\ \{d_1^i\} \tag{6.37}$$

where

$$[r^i] = [T^i_{12}]^{-1} [B^i]^{-1} \tag{6.38}$$

$$[s^i] = -[T^i_{12}]^{-1} [T^i_{11}] \tag{6.39}$$

Expanding Eq. (6.39)

$$\begin{Bmatrix} M^i_{x1} = k_\phi \phi^i_1 \\ 0 \\ 0 \\ V^i_{y1} \\ V^i_{z1} \\ V^i_{x1} \end{Bmatrix} = \left[\begin{array}{c|c} r_{11} & r_{12} \\ \hline r_{21} & r_{22} \end{array}\right] \begin{Bmatrix} l_{d2} \\ \hline r_{d2} \end{Bmatrix}$$

$$+ \left[\begin{array}{c|c} s_{11} & s_{12} \\ \hline s_{21} & s_{22} \end{array}\right] \begin{Bmatrix} 0 \\ 0 \\ 0 \\ \hline \varepsilon^i_1 \\ \xi^i_1 \\ \phi^i_1 \end{Bmatrix}$$

Extracting and rewriting the top three equations of the above equation yields

$$\begin{bmatrix} 0 & 0 & k_\phi \\ 0 & 0 & 0 \\ 0 & 0 & 0 \end{bmatrix} \begin{Bmatrix} \varepsilon_1^i \\ \xi_1^i \\ \phi_1^i \end{Bmatrix} = [r_{11}] \{l_{d_2}\} + [r_{12}] \{r_{d_2}\}$$

$$+ [s_{12}] \begin{Bmatrix} \varepsilon_1^i \\ \xi_1^i \\ \phi_1^i \end{Bmatrix} \qquad (6.40)$$

From Eq. (6.40)

$$\begin{Bmatrix} \varepsilon_1^i \\ \xi_1^i \\ \phi_1^i \end{Bmatrix} = [p]^{-1} [r_{11}] \{l_{d_2}\} + [p]^{-1} [r_{12}] \{r_{d_2}\} \qquad (6.41)$$

where [p] is defined in Eq. (4.29)

From Eqs. (6.41) and the boundary condition equation (6.26) for spring restrained branches

$$\{d_1^i\} = [a^i] \{d_2\} \qquad (6.42)$$

where

$$[a^i] = \begin{bmatrix} 0 & | & 0 \\ - - - - - & | & - - - - - \\ [p]^{-1}[r_{11}] & | & [p]^{-1}[r_{12}] \end{bmatrix}$$

Substituting Eq. (6.42) into Eq. (6.41) yields

$$\{f_1^i\} = [r^i]\ \{d_2\} + [s^i]\ [a^i]\ \{d_2\} \tag{6.43}$$

Substituting Eqs. (6.42) and (6.43) into Eq. (6.24) yields

$$\{f_2^i\} = [k^i]\ \{d_2\} \tag{6.44}$$

where

$$[k^i] = [T_{22}^i]\ [r^i] + ([T_{22}^i]\ [s^i] + [T_{21}^i])\ [a^i] \tag{6.45}$$

Equilibrium is enforced by substituting Eq. (6.44) into Eq. (3.4), giving

$$\{f_2\} = [D]\ \{d_2\} \tag{6.46}$$

where

$$[D] = \sum_{i=1}^{n} [A^i]\ [k^i] \tag{6.47}$$

Substituting Eq. (6.46) into Eq. (6.20) yields

$$\{f_3\} = ([T_{21}] + [T_{22}]\ [D])\ \{d_2\} \tag{6.48}$$

The boundary condition for the blade tip is given by

$$\{f_3\} = \{0\} \tag{6.49}$$

Application of this boundary condition to equation (6.48) yields

$$([T_{21}] + [T_{22}]\,[D])\,\{d_2\} = \{0\} \tag{6.50}$$

For nontrivial solutions of $\{d_2\}$, the determinant of the coefficient matrix should be zero and this condition yields the following frequency equation to determine the natural frequencies of the multiple branch blades.

$$\det([T_{21}] + [T_{22}]\,[D]) = 0 \tag{6.51}$$

For single branch blades, the boundary conditions are assumed as shown below.

$$x = 0: \qquad u_1 = w_1 = v_1 = \varepsilon_1 = \xi_1 = 0 \qquad \phi_1 = M_{x_1}/k_\phi \tag{6.52}$$

$$x = R: \qquad \{f_3\} = \{0\} \tag{6.53}$$

The equilibrium and compatibility matrices become identity matrices and this yields

$$\{d_2\} = \{d_2^1\} = [T_{11}^1]\,\{d_1\} + [\,T_{12}^1]\,\{f_1\} \tag{6.54}$$

$$\{f_2\} = \{f_2^1\} = [T_{21}^1]\,\{d_1\} + [\,T_{22}^1\,]\,\{f_1\} \tag{6.55}$$

Substituting Eqs. (6.54) and (6.55) into Eq. (6.20) yields

$$\{f_3\} = [A]\,\{d_1\} + [B]\,\{f_1\} \tag{6.56}$$

(6.52)

where

$$[A] = [T_{21}]\,[T^{1}_{11}] + [T_{22}]\,[T^{1}_{21}] \tag{6.57}$$

$$[B] = [T_{21}]\,[T^{1}_{12}] + [T_{22}]\,[T^{1}_{22}] \tag{6.58}$$

Application of the boundary condition equations (6.52) and (6.53) to equation (6.56) gives

$$\{0\} = [A] \begin{Bmatrix} 0 \\ 0 \\ 0 \\ 0 \\ 0 \\ \phi \end{Bmatrix}_1 + [B] \begin{Bmatrix} M_x = k_\phi \phi \\ M_z \\ M_y \\ V_y \\ V_z \\ V_x \end{Bmatrix}_1 \tag{6.59}$$

From Eq. (6.59)

$$[D]\,\{f_1\} = \begin{Bmatrix} 0 \\ 0 \\ 0 \\ 0 \\ 0 \\ 1 \end{Bmatrix} \phi_1 \tag{6.60}$$

where

$$[D] = -[A]^{-1}[B]$$

Extracting the last row of the above equation yields

$$D_{6,1}k_\phi\phi_1 + \lfloor D_{6,2}\ D_{6,3}\ D_{6,4}\ D_{6,5}\ D_{6,6} \rfloor \begin{pmatrix} M_z \\ M_y \\ V_y \\ V_z \\ V_x \end{pmatrix}_1 = \phi_1 \qquad (6.61)$$

Rearrange Eq. (6.61) as

$$\phi_1 = \lfloor a_1\ a_2\ a_3\ a_4\ a_5\ a_6 \rfloor \{f_1\} \qquad (6.62)$$

where

$$a_1 = 0 \text{ and } a_j = \frac{D_{6,j}}{D_{6,1}k_\phi\phi - 1}\ ,\ j = 2 \text{ to } 6$$

Substituting Eq. (6.42) into Eq. (6.60) yields

$$([D] - [A])\{f_1\} = \{0\} \qquad (6.63)$$

where

$$\{A\} = \begin{Bmatrix} 0 \\ 0 \\ 0 \\ 0 \\ 0 \\ 1 \end{Bmatrix} \begin{bmatrix} a_1 & a_2 & a_3 & a_4 & a_5 & a_6 \end{bmatrix}$$

For nontrivial solution of $\{f_1\}$, the determinant of the coefficient matrix of Eq. (6.63) should be zero and this condition yields the following frequency equation to determine the natural frequenices of the single branch blade.

$$\det([D] - [A]) = 0 \tag{6.64}$$

6.4 Mode Shapes

A mode shape may be defined as the shape corresponding to a specific frequency in which the elastic and inertial forces are in equilibrium. The formulation for calculating the fully coupled flap, lag and pitch mode shapes follows.

$$\left\{ \begin{array}{c} d_2 \\ - - - \\ f_2 \end{array} \right\} = \left[\begin{array}{c|c} \bar{T}_{11} & \bar{T}_{12} \\ - - - & - - - \\ \bar{T}_{21} & \bar{T}_{22} \end{array} \right] \left\{ \begin{array}{c} d_3 \\ - - - \\ f_3 \end{array} \right\} \tag{6.65}$$

where

$$[\bar{T}] = [T]^{-1}$$

From the above equation, the displacement vector at the clevis is as shown below by virtue of the boundary condition at the blade tip $\{f_3\} = \{0\}$,

$$\{d_2\} = [\bar{T}_{11}]\,\{d_3\} \tag{6.66}$$

Substituting Eq. (6.66) into Eq. (6.48) yields

$$\{f_3\} = [C]\,\{d_3\} \tag{6.67}$$

where

$$[C] = ([T_{11}] + [T_{22}]\,[D])\,[\bar{T}_{11}]$$

Assuming $w_3 = 1$ arbitrarily and rewriting rows 2 to 6 of Eq. (6.67) gives

$$\begin{bmatrix} C_{2,1} & C_{2,3} & C_{2,4} & C_{2,5} & C_{2,6} \\ C_{3,1} & C_{3,3} & C_{3,4} & C_{3,5} & C_{3,6} \\ C_{4,1} & C_{4,3} & C_{4,4} & C_{4,5} & C_{4,6} \\ C_{5,1} & C_{5,3} & C_{5,4} & C_{5,5} & C_{5,6} \\ C_{6,1} & C_{6,3} & C_{6,4} & C_{6,5} & C_{6,6} \end{bmatrix} \begin{Bmatrix} u_3 \\ v_3 \\ \varepsilon_3 \\ \xi_3 \\ \phi_3 \end{Bmatrix} = \begin{Bmatrix} -C_{2,2} \\ -C_{3,2} \\ -C_{4,2} \\ -C_{5,2} \\ -C_{6,2} \end{Bmatrix} \tag{6.68}$$

By solving the above equation, $u_3, v_3, \varepsilon_3, \xi_3$, and ϕ_3 are known and together with $w_3 = 1$ the entire blade tip deflection $\{d_3\}$ is known. Once $\{d_3\}$ is known, the state vector at the clevis can be determined ferom Eq. (6.65) as shown below.

$$\left\{\begin{array}{c} d_2 \\ - - - \\ f_2 \end{array}\right\} = \left[\begin{array}{c} \bar{T}_{11} \\ - - - \\ \bar{T}_{21} \end{array}\right] \{d_3\} \tag{6.69}$$

Once the state vector at the clevis is known, the deflection vectors in the blade and the branches can be obtained as follows.

Blade: By definition of the transfer matrix, the state vector at any location x is given by

$$\left\{\begin{array}{c} d_x \\ - - - \\ f_x \end{array}\right\} = \left[\begin{array}{c|c} T_{11} & T_{21} \\ - - - & - - - \\ T_{21} & T_{22} \end{array}\right]_x \left\{\begin{array}{c} d_2 \\ - - - \\ f_2 \end{array}\right\} \tag{6.70}$$

From the above equation

$$\{d_x\} = [T_{11}]_x \{d_2\} + [T_{12}]_x \{f_2\} \tag{6.71}$$

Branches: By definition of the transfer matrix, the state vector at any location x in the branch is given by

$$\left\{\begin{array}{c} d_x^i \\ - - - \\ f_x^i \end{array}\right\} = \left[\begin{array}{c|c} T_{11}^i & T_{12}^i \\ - - - & - - - \\ T_{21}^i & T_{22}^i \end{array}\right] \left\{\begin{array}{c} d_1^i \\ - - - \\ f_1^i \end{array}\right\} \tag{6.72}$$

For clamped root branches the following equation can be extracted from Eq. (6.72) by virtue of the boundary condition deflections $\{d_1\} = \{0\}$ at the root.

$$\{d_x^i\} = [T_{12}^i]\ \{f_1^i\} \tag{6.73}$$

For spring restrained root branches the equation remains as

$$\{d_x^i\} = [T_{11}^i]\ \{d_1^i\} + [T_{12}^i]\ \{f_1^i\} \tag{6.74}$$

Eq. (6.31) provides $\{f_1^i\}$ for clamped branches, and Eqs. (6.42) and (6.43) provide $\{d_1^i\}, \{f_1^i\}$ for spring restrained branches.

For single branch blades Eq. (6.63) can be solved for $\{f_1\}$ assuming $V_Z = 1$ arbitrarily, and then ϕ_1 can be comnputed from Eq. (6.61).

branch: $$\{d_x\} = [T_{11}^1]\ \{d_1\} + [T_{12}^1]\ \{f_1\} \tag{6.75}$$

blade: $$\{d_x\} = [T_{11}]\ \{d_2\} + [T_{12}]\ \{f_2\} \tag{6.76}$$

7. AEROELASTIC STABILITY CHARACTERISTICS

7.1 Equations for Aeroelastic Stability

The perturbation equations (5.1) - (5.12) are specialized with a transformation to the frequency domain to determine the equations governing the aeroelastic stability characteristics of branched blades. The transformation is accomplished by substituting

$$\{z^p(x,t)\} = Z^p(x)\}\, e^{\lambda t} \tag{7.1}$$

where λ is complex and equal to $\sigma + i\omega$. (Note that for free vibration λ was simply equal to $i\omega$.) The resulting equations are (superscripts p omitted)

$$u' = -\varepsilon_o\varepsilon - \xi_o\xi + V_x/EA \tag{7.2}$$

$$w' = \varepsilon \tag{7.3}$$

$$v' = \xi \tag{7.4}$$

$$\begin{aligned}\varepsilon' = {} & -a_1 M_{x_o}\varepsilon + a_1 M_{x_o}\xi - (2a_1 M_{y_o} + a_4 M_{z_o})\phi \\ & + (-a_1\varepsilon_o + a_3\xi_o)M_x + (a_1 - a_4\phi_o)M_z \\ & - (a_3 + 2a_1\phi_o)M_y\end{aligned} \tag{7.5}$$

$$\begin{aligned}\xi' = {} & -a_2 M_{x_o}\varepsilon + a_1 M_{x_o}\xi - (2a_1 M_{z_o} - a_4 M_{y_o})\phi \\ & + (-a_2\varepsilon_o + a_1\xi_o)M_x + (a_2 - 2a_1\phi_o)M_z \\ & - (a_1 - a_4\phi_o)M_y\end{aligned} \tag{7.6}$$

$$\phi' = (1/GJ)(M_{z_o}\varepsilon + M_{y_o}\xi + M_x + \varepsilon_o M_z + \xi_o M_y \qquad (7.7)$$

$$\begin{aligned} M_x' = {} & -2me\Omega\sin\theta\lambda u + me(\cos\theta - \phi_o \sin\theta)\lambda^2 w \\ & - me(\sin\theta + \phi_o \cos\theta)\lambda^2 - \Omega^2)v \\ & + 2\Omega m(k_{m2}^2 \sin^2\theta + k_{m1}^2 \cos^2\theta)\lambda\varepsilon + V_{y_o}\varepsilon \\ & + 2\Omega m(k_{m2}^2 - k_{m1}^2)\cos\theta\sin\theta\lambda\xi - V_{z_o}\xi \\ & + \{mk_{m2}^2\lambda^2 + \Omega^2 m(k_{m2}^2 - k_{m1}^2)(\cos 2\theta - \phi_o \sin 2\theta) \\ & + me\Omega^2 v_o \cos\theta\}\phi + \varepsilon_o V_y - \xi_o V_z - M_e \end{aligned} \qquad (7.8)$$

$$M_z' = 2\Omega me\Omega\cos\theta\lambda v + V_{x_o}\xi - me\Omega^2 x\sin\theta\phi - V_y + \xi_o V_x \qquad (7.9)$$

$$M_y' = 2\Omega me\Omega\sin\theta\lambda v - V_{x_o}\varepsilon - me\Omega^2 x\cos\theta\phi + V_z - \varepsilon_o V_x \qquad (7.10)$$

$$\begin{aligned} V_y' = {} & 2\Omega\lambda u + m(\lambda^2 - \Omega^2)v - 2\Omega me\lambda\sin\theta\varepsilon \\ & - 2\Omega me\lambda\cos\theta\xi + me\sin\theta(\Omega^2 - \lambda^2)\phi \\ & - L_v - 2m\Omega\beta_{pc}\lambda w \end{aligned} \qquad (7.11)$$

$$V_z' = m\lambda^2 w + me\lambda^2\cos\theta\phi - L_w + 2m\Omega\beta_{pc}v \qquad (7.12)$$

$$V_x' = m(\lambda^2 - \Omega^2)u - 2\Omega m\lambda v \qquad (7.13)$$

where

$$L_v = k_4[-\Omega x v_{i_o}\phi - \{2\Omega x k_2 + (\theta+\phi_o)v_{i_o}\}\lambda v + \{2v_{i_o} - \Omega x(\theta+\phi_o)\lambda w - k_1 v_{i_o}(\lambda\phi+\Omega\varepsilon) - \Omega k_1(\varepsilon_o + \beta_{pc})\lambda w \quad (7.14)$$

$$L_w = k_4[\Omega^2 x^2\phi - \Omega^2 x(v_o\varepsilon+\varepsilon_o v) - \Omega^2 x\beta_{pc}v + k_1\Omega^2 x\varepsilon + \{2\Omega x(\theta+\phi_o) - v_{i_o} + \Omega k_1(\varepsilon_o+\beta_{pc})\}\lambda v - \Omega x\lambda w + k_1\Omega x\lambda\phi] \quad (7.15)$$

$$M_e = k_3 L_w - k_4 c^2[\Omega x\lambda\phi + \Omega^2 x\varepsilon + \Omega\lambda(\varepsilon_o+\beta_{pc})v] \quad (7.16)$$

and

$k_1 = c(1-e)/2$ $\qquad$ $k_3 = ce/2$

$k_2 = c_d/a$ $\qquad$ $k_4 = \rho ac/2$

7.2 Stability Eigenvalues

Equations (7.2)-(7.13) are linear homogeneous equations like the free vibration equations (6.1)-(6.12), and calculation of the complex transfer matrices proceeeds similarly for the branches and blade. Equations (7.2)-(7.13) can be arranged into a matrix differential equation

$$\{z(x)\}' = [A(x)]\{z(x)\} \quad (7.14)$$

where [A(x)] is now complex. The transfer matrix for the above system is given by solving the following equations

$$[T(x)]' = [A(x)]\,[T(x)] \tag{7.15}$$

$$[T(0)] = [I] \tag{7.16}$$

Once the transfer matrices are known for the blade and branches a stability determinant is formulated. The stability determinant is of the same form as the frequency determinant (equation 6.47) and is given by

$$\det([T_{21}] + [T_{22}]\,[D]) = 0 \tag{7.17}$$

where [D] is defined with equation (6.43).

The eigenvalues of the stability determinant are complex whereas the eigenvalues of the frequency determinant are real. Thus λ in equations (7.2) - (7.16) takes complex values. The eigenvalues of the stability determinant are calculated by Muller's method [42] for determining complex roots, whereas the eigenvalues of the frequency determinant are calculated by a frequency scanning technique.

Stability of the branched blade is inferred by examining the sign of σ (the real part of λ). If σ is positive then it can be seen from (7.1) that the perturbation state vector increases exponentially with time and thus the system is unstable. If σ is negative, then the perturbation state vector decreases with time and eventually damps out. In this case the system is stable.

8. NUMERICAL RESULTS AND DISCUSSION

8.1 Computer Program

A comprehensive computer program is developed to implement the formulation presented in the preceding chapters. The program determines the following for a branched blade with up to three branches:

1. Natural frequencies and mode shapes about the undeformed position
2. Steady state nonlinear deflections of the blade and branches
3. Natural frequencies and mode shapes about the steady state deformed position
4. Complex stability eigenvalues

Additionally, the program features fully coupled nonlinear flapwise bending, chordwise bending, torsion and axial extensions. It can also handle noncoincident mass, elastic and aerodynamic center axes with nonuniform property distributions in both the blade and branches. The code is lengthy (approximately 4000 lines) and thus is included in a separate volume.

The program is based on a continuous system model, with transfer matrices calculated by a fourth order Runge–Kutta integration scheme. It should be noted that if a discrete model is used to compute the transfer matrices the formulation is still valid.

The transfer matrices based on the discrete model can be used in place of those computed based on the continuous system model.

8.2 Validation of Nonlinear Formulation – Single Branch Blade

To demonstrate the extension of the transfer matrix method to nonlinear problems, the conventional single–branch rotor blade model considered in reference [40] is analyzed first. The data of the model is shown in Table 8.1.

The natural frequencies (both rotating and nonrotating) are given in Table 8.2. Nonrotating frequencies about the initial undeformed state are computed using the present method and closed form analytical expressions (see Appendix B). The rotating blade frequencies are shown about both the initial undeformed position and the nonlinear steady deformed position. The flap frequencies are strongly effected by rotation due to added stiffness coming from centrifugal effects. Chord and torsion frequencies are much less sensitive to rotation. The frequencies about the deformed state are seen to be close to those about the initial undeformed state.

The steady state nonlinear tip deflections are given in Table 8.3. These trim tip deflections are compared graphically with the results of reference [39] in Figure 8.1, and the agreement is quite good. The Newton–Raphson iteration scheme developed for the nonlinear distributed system equations is employed to obtain the convergence. The efficiency of the scheme is indicated in Table 8.4

Table 8.1

Data for conventional blade

C/R = 40 in	$k_{m_2} = 0$
$\theta = 0.0^o$	$k_{m_2}/2 = 0.025$
$\beta_{pc} = -2.8648^o$ to 5.7296^o	$(k_A/k_m)^2 = 1.5$
$\bar{\omega}_w = 1.15$	a = 2 π per rad
$\bar{\omega}_v = 1.50$	b = 4
$\bar{\omega}_\phi = 5.0$	$c_{d_o}/a = 0.01/2\pi$
$\gamma = (3\rho_{aCR}/m) = 5$	$\theta_{rc} = 0.0^o$ to 28.6479^o
e/R = 0.0	

Table 8.2

Natural frequencies (rad/sec), single branch blade

Mode	Initial state			Deformed state
	$\Omega = 0$	$\bar{\Omega}^2 = 9.3456$		$\bar{\Omega}^2 = 9.4356$
	Present Method	Analytical		$\beta_{rc} = 0.3$ rad
1	3.3813 F	3.3810	9.1576	8.5005
2	11.4324 C	11.4314	11.9370	12.0323
3	21.1905 F	21.1898	29.3043	28.9895
4	37.6596 T	37.6601	39.7894	40.3584
5	59.3348 F	59.3381	68.1363	67.5846
6	71.6468 C	71.6443	74.0281	73.8076
7	112.9801 T	112.9803	116.4039	117.2911
8	116.2750 F	116.2725	125.6590	124.7716
9	188.3004 T	188.3004	193.6040	194.0339
10	192.1118 F	192.2055	201.9584	200.5757

F = Predominantly flapwise
C = Predominantly chordwise
T = Predominantly torsion

Table 8.3

Steady state deflections, conventional blade

Precone β_{pc} (rad)	Root Collective θ_{rc} (rad)	$\bar{w}_{o_{tip}}$	$\bar{v}_{o_{tip}}$	$\phi_{o_{tip}}$
-0.05 (-2.86°)	0.0	0.4079×10^{-1}	-0.5266×10^{-3}	0.2027×10^{-3}
	0.1 (5.73°)	0.6197×10^{-1}	-0.6360×10^{-2}	-0.4760×10^{-2}
	0.2	0.9527×10^{-1}	-0.1944×10^{-1}	-0.9353×10^{-2}
	0.3 (17.19°)	0.1329	-0.4109×10^{-1}	-0.1391×10^{-1}
	0.4	0.1721	-0.7189×10^{-1}	-0.2001×10^{-1}
	0.5 (28.65°)	0.2096	-0.1110	-0.3180×10^{-1}
0.00	0.0	0.0000	-0.5222×10^{-3}	0.0000
	0.1	0.2150×10^{-1}	-0.2942×10^{-2}	-0.4693×10^{-2}
	0.2	0.5554×10^{-1}	-0.1272×10^{-1}	-0.8666×10^{-2}
	0.3	0.9466×10^{-1}	-0.3145×10^{-1}	-0.1174×10^{-1}
	0.4	0.1366	-0.6024×10^{-1}	-0.1469×10^{-1}
	0.5	0.1790	0.9938×10^{-1}	-0.2022×10^{-1}
0.05	0.0	-0.4079×10^{-1}	-0.5266×10^{-3}	0.2027×10^{-3}
	0.1	-0.1935×10^{-1}	0.5137×10^{-3}	-0.5085×10^{-2}
	0.2	0.1503×10^{-1}	-0.5813×10^{-2}	-0.8956×10^{-2}
	0.3	0.5516×10^{-1}	-0.2128×10^{-1}	-0.1120×10^{-1}
	0.4	0.9922×10^{-1}	-0.4746×10^{-1}	-0.1202×10^{-1}
	0.5	0.1454	-0.8553×10^{-1}	-0.1313×10^{-1}
0.05	0.0	-0.8157×10^{-1}	-0.5398×10^{-3}	-0.4070×10^{-3}
	0.1	-0.6058×10^{-1}	0.3977×10^{-2}	-0.5938×10^{-2}
	0.2	-0.2628×10^{-1}	0.1234×10^{-2}	-0.1022×10^{-1}
	0.3	0.1440×10^{-1}	-0.1069×10^{-1}	-0.1224×10^{-1}
	0.4	0.6005×10^{-1}	-0.3375×10^{-1}	-0.1159×10^{-1}
	0.5	0.1094	-0.6994×10^{-1}	-0.9264×10^{-2}

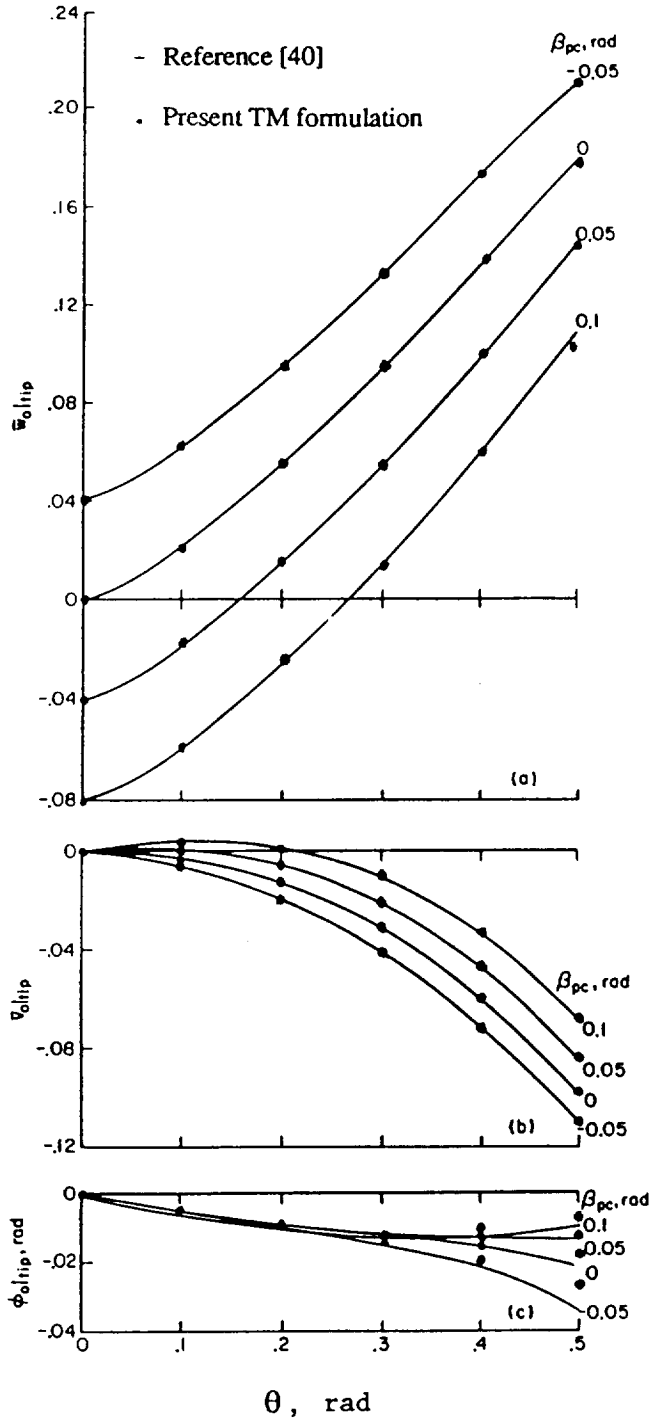

Figure 8.1 Comparison of Steady State Deflections

Table 8.4

Convergence of nonlinear steady state trim (tip deflections)

$\beta_{pc} = 0.05$ (2.86°), $\theta_{rc} = 0.3$ rad (17.19°)

State variable	Starting solution $z^{(1)}(x)$	Starting solution $z^{(2)}(x)$	I iteration	II iteration	III iteration
u	0.3946×10^{-6}	-0.1913×10^{-2}	-0.2023×10^{-2}	-0.2007×10^{-2}	-0.2007×10^{-2}
w	0.5140×10^{-1}	0.5563×10^{-1}	0.5516×10^{-1}	0.5516×10^{-1}	0.5516×10^{-1}
v	-0.2037×10^{-1}	-0.2145×10^{-1}	-0.2128×10^{-1}	-0.2128×10^{-1}	-0.2128×10^{-1}
ε	0.7444×10^{-1}	0.7972×10^{-1}	0.7912×10^{-1}	0.7912×10^{-1}	0.7912×10^{-1}
ξ	-0.2868×10^{-1}	-0.2990×10^{-1}	-0.2967×10^{-1}	-0.2967×10^{-1}	-0.2967×10^{-1}
ϕ	-0.1406×10^{-1}	-0.1034×10^{-1}	-0.1121×10^{-1}	-0.1120×10^{-1}	-0.1120×10^{-1}

which shows the nonzero elements (deflections) of {z} at the blade tip. The first and second columns of this table are given by equations (4.1a) and (4.1b) respectively. The third, fourth and fifth columns are the first, second and third Newton–Raphson iterative solutions respectively computed using equations (4.7). All the blade tip motions are converged to four significant figures.

The complex stability eigenvalues are determined from perturbations about the nonlinearly deformed steady state position. The stability eigenvalues obtained using the present method are compared with the results obtained in references [40] and [44] in Table 8.5. Since the real parts of the eigenvalues are negative for all the modes (flap, lag and torsion) the perturbation motion damps out and the system is stable. The flap and torsional motions have a much larger stability margin than the lag motion since the real parts of those eigenvalues are much larger negative numbers than the real part of the lag stability eigenvalue. It is also interesting to note that the imaginary parts of the stability eigenvalues in Table 8.5 are quite close in value to the natural frequencies computed about the non-linearly deformed steady deformed position (Table 8.2). Since the imaginary part of the stability eigenvalue represents the damped natural frequency and it is quite close to the undamped natural frequency it is clear that there is very little damping in this system.

Table 8.5

Comparison of stability eigenvalues, conventional blade

	θ_{rc} = 0.3 rad (17.19°), β_{pc} = 0.0 rad		
	Present TM Formulation (rad/sec)	Ref. 40	Ref. 44
Flap	-2.2509 + 7.3895i	-2.2449 + 7.5554i	-2.2194 + 7.5957i
Lead-lag	-0.4851 + 12.5397i	-0.5029 + 12.5915i	-0.5308 + 12.4642i
Torsion	-2.7870 + 40.23271i	-2.7932 + 39.1123i	-2.7780 + 40.2057i

8.3 Validation of Multiple Branch Formulation

The formulation for multiply-branched blades is validated by performing the calculations for the twin beam model considered by Sivaneri and Chopra [33]. The data for the twin beam model are shown in Table 8.6.

The rotating natural frequencies are shown in Table 8.7. Frequencies about both the initial state and the nonlinearly deformed trim state are presented. Those computed by the present method agree well with Sivaneri and Chopra's results [33].

The nonlinear steady state trim deflections computed from the present method are compared with those obtained in [33] in Table 8.8. Minor differences in the trim deflection are attributable to differences in input data in the axial stiffnesses of the two load path branches at the blade root. Specifically, the axial stiffnesses of these members significantly effects the in–plane bending stiffness due to load path offsets. This parameter was not explicitly defined by Sivaneri and Chopra in [33] and thus may differ from that used for the present calculations.

The stability eigenvalues for both methods are compared in Table 8.9. Examination of the real parts of the flap and torsion eigenvalues shows good agreement, with both methods indicating a negative sign and subsequently stable flap and torsion motions. However both methods result in a lag eigenvalue with a positive real part. This indicates that the lag mode of the system is unstable, and any perturbation motion will grow with time. The difference in

Table 8.6

Data for the branched blade

Blade	2 Identical Load Paths
$C/R = \pi/40$	$\theta = 0.0$
Blade/R = 0.75	$\beta_{pc} = 0.05$ rad = 2.8648°
Flexure/R = 0.25	$EI_y/\Omega^2 m_o R^4 = 0.007243$
θ = 12.7183 (constant)	$EI_z/\Omega^2 m_o R^4 = 0.083454$
$\beta_{pc} = 0.05$ rad = 2.8648°	$GJ/\Omega^2 m \cdot R = 0.000925$
$EI_y/\Omega^2 m_o R^4 = 0.014486$	$k_{m_1}/R = 0.0$
$EI_z/\Omega^2 m_o R^4 = 0.166908$	$EA/\Omega^2 m\, R^4 = 0.0604646$
$GJ/\Omega^2 m_o R^4 = 0.0004625$	$k_{m_2}/R = 0.0125$
$m/m_o R^4 = 1$	$k_A/k_m = 0.5$
e/R = 0.0	e/R = 0.0
$\bar{k}_{m_1} = 0.0$	$m/m_o = 0.5$
$\bar{k}_{m_2} = 0.025$	
$(k_A/k_m)^2 = 1.5$	Clevis Geometry for Twinbeam Model
$EA/\Omega^2 n_o R^4 = -0.1209293$	
$\sigma = 0.1$	$h_{y_1} R/C = 16$
a = 6.0 per rad	$h_{z_1} = 0.0$ in
$c_{d_o} = 0.0095$	$h_{y_2} R/C = 16$
$\theta_{rc} = 0.0°$	$h_{z_2} = 0.0$ in

Table 8.7
Natural frequencies (ω/Ω), twin branched blade

Initial State		Trimmed state	
$C_T/\sigma = 0$		$C_T/\sigma = 0.1$, $\beta_{pc} = 0.05$ (2.86°); $\gamma = 5.0$	
Present Formulation	Ref. 33	Present Formulation	Ref. 33
1.150	1.149	1.14888	1.14974
1.874	1.870	1.77702	1.77961
2.908	2.910	2.90542	2.88141
3.675		3.78192	
7.624		7.62226	
8.536		8.41963	
10.007		10.14406	
11.233		11.23863	
15.224		15.22107	
15.7355		15.77955	

Table 8.8

Nonlinear steady state tip deflections, twin branched blade

$C_T/\sigma = 0.1$, $\beta_{pc} = 0.05$ (2.86°); $\gamma = 5.0$, $\omega_w/\Omega = 1.15$, $\omega_v/\Omega = 1.87$

$\omega_\phi/\Omega = 2.91$, zero inboard pitch

	$\bar{u}_o$	$\bar{w}_o$	$\bar{v}_o$	$\bar{\phi}_o$
Present TM Formulation	0.001548	0.01595	-0.004130	-0.02970
Ref. 33	0.01613	0.011213	-0.003750	-0.030735

Table 8.9

Stability eigenvalues, twin branched blade

	Flap (λ/Ω)	Lead-lag (λ/Ω)	Torsion (λ/Ω)
Present TM Formulation	-0.34539 + 1.03535i	0.01102 + 1.76109i	-0.40113 + 2.92296i
Ref. 33	-0.35267 + ———i	0.00445 + 1.76i	-0.38119———i

magnitude of the real part of the lag eigenvalues can be due to differences in the trim position the stability is computed about.

9. CONCLUDING REMARKS

The objective of the present research is to extend the transfer matrix method to a new class of problems and generate numerical results to verify the concepts developed. Herein a direct transfer matrix method is developed to determine the dynamic characteristics of branched autonomous nonlinear rotor blades. The new features of the present formulation compared to traditional transfer matrix methods are its ability to treat nonlinear boundary value problems (using a Newton–Raphson iteration scheme developed for distributed systems) and treat multiply branched distributed systems. In the case of the multiply branched rotor systems, a rapid iterative scheme is employed for the estimation of the tension coefficients in the blade root branches.

The analysis is coded in a FORTRAN computer program, which calculates (1) natural frequencies and mode shapes about both the initial undeformed and deformed trim states, (2) nonlinear steady state deflections corresponding to the hover trim state and (3) aeroelastic stability characteristics of single and multiple–branch rotor blades. Throughout the actual calculations, the order of the matrices involved is only six by six so the method is computationally efficient.

The analysis is applied to two different rotor configurations. A conventional single–branch blade is considered to validate the nonlinear portion of the analysis. The single–branch blade

frequencies, nonlinear trim deflections, and complex stability eigenvalues presented provide excellent correlation with the known results. A twin–branch blade is also analyzed and its frequencies, nonlinear trim deflections and complex stability eigenvalues are in agreement with the published data.

The numerical results thus validate the advancement of the transfer matrix method to treat nonlinear distributed boundary value problems with multiple branches.

The extended transfer matrix method has a great potential for use in several classes of engineering problems because of its computational efficiency. With computer speed roughly doubling every eighteen months, it is conceivable to tackle system optimization or near real–time system simulation with an unprecedented level of modeling sophistication. This could radically change the way current designs are developed, because it would allow an designer to evaluate many more designs and thus explore a much bigger region of the design space.

The next logical step for the rotorcraft application is to attack the forward flight problem. The primary complication in forward flight is the changed nature of the governing equations. In particular, the aerodynamic lift, drag and moment vary in a periodic fashion around the azimuth. This results in a set of nonlinear partial differential equations in space and time with periodic coefficients. In hover, the equations have constant coefficients and by assuming the motions are simple harmonic motions it is possible to reduce the

partial differential equations in space and time to ordinary differential equations in space.

This approach is not viable for the forward flight equations. There are several alternatives for computing the solution of the periodic forward flight equations.

1. The free vibration problem is solved and the modes (eigenfunctions if using a continuous system model, eigenvectors if using a discrete system model) are used to reduce the partial differential equations to a set of ordinary differential equations in generalized time coordinates. The solution is then obtained by integrating the ordinary differential equations in generalized coordinates and constructing the complete solution via modal transformations. In this approach the transfer matrix method is only used to solve the free vibration problem.
2. The second approach is known as harmonic analysis. In this approach the rotor blade is not modeled as a continuous system but is discretized into a finite set of elements. The state vector at a given radial location undergoes periodic variation as it moves around the azimuth. Thus the motion at that station can be expanded in a Fourier series which has as its frequencies multiples of rotor speed. For an infinite Fourier series the result is an infinite set of algebraic equations, with one set of algebraic equations each for the zeroth, first, second, etc. harmonic coefficients in the Fourier

series. In practice the Fourier series are truncated and so the result is a finite set of algebraic equations which are solved with routine linear algebra techniques. This approach lends itself readily to the transfer matrix method since transfer matrices can be used to relate the harmonic coefficients at different radial locations.

Both approaches are adequate for obtaining solutions to the forward flight equations. However when using the modal approach some approximations are incurred, and the level of accuracy is dependent on how many modes are used. Highly nonlinear systems are unwieldy to analyze using modes, and usually require careful formulation and a large number of modes for reasonable accuracy. The accuracy of the combined Fourier series and transfer matrix approach is only dependent on the number of terms retained in the series, and nonlinear systems are easier to model. For these reasons the second approach is currently under development at Boeing Helicopters. It is the foundation for the work in progress described in reference [45].

REFERENCES

1. H. Holzer, Die Berechnung der Drehschwingungen. Springer-Verlag, Berlin (1921). Republished by J. W. Edwards Inc., Ann Arbor, Michigan (1948).

2. N. O. Myklestad, New Method of Calculating Natural Modes of Coupled Bending-Torsion Vibration of Beams. Transactions of the American Society of Mechanical Engineers 67, 61-67 (1945).

3. W. T. Thomson, Matrix Solution of Vibration of Nonuniform Beams. Journal of Applied Mechanics 17, 337-339 (1950).

4. C. T. Molloy, Four Pole Parameters in Vibration Analysis. Colloquium on Mechanical Impedance Methods for Mechanical Vibrations, Applied Mechanics Division, ASME, 53-68 (1958).

5. E. C. Pestel and F. A. Leckie, Matrix Methods in Elastomechanics. McGraw-Hill Book Company, Inc., New York (1963).

6. S. Rubin, Transmission Matrices for Vibration and their Relation to Admittance and Impedance. Journal of Engineering for Industry, Transactions of the American Society of Mechanical Engineers 86, 9-21.

7. S. Rubin, Review of Mechanical Immitance and Transmission Matrix Concepts. Journal of the Acoustical Society of America 41, 1171-1179.

8. W. P. Targoff, The Associated Matrices of Bending and Coupled Bending-Torsion Vibrations. Journal of Aeronautical Sciences 14, 579-582 (1947).

9. Y. K. Lin, Probabilistic Theory of Structural Dynamics. McGraw-Hill Book Company, Inc., New York (1967).

10. Y. K. Lin and T. J. McDaniel, Dynamics of Beam-Type Periodic Structures. Journal of Engineering for Industry 91, 1133-1141 (1969).

11. C. A. Mercer and C. Seavey, Prediction of Natural Frequencies and Normal Modes of Skin-Stringer Panel Rows. Journal of Sound and Vibration 6, 149-162 (1967).

12. D. J. Mead, Vibration Response and Wave Propagation in Periodic Structures. Journal of Engineering for Industry 93, 783-792 (1971).

13. D. J. Mead and G. Sen Gupta, Propagation of Flexural Waves in Infinite, Damped Rib-Skin Structures. USAF Report AFML-TR-70-13 (1970).

14. J. P. Henderson and T. J. McDaniel, The Analysis of Curved Multi-Span Structures. Journal of Sound and Vibration 18, 203-219 (1971).

15. T. J. McDaniel, Dynamics of Circular Periodic Structures. Journal of Aircraft 8, 143-149 (1971).

16. T. J. McDaniel and J. D. Logan, Dynamics of Cylindrical Shells with Variable Curvature. Journal of Sound and Vibration 19, 39-48 (1971).

17. V. R. Murthy and N. C. Nigam, Dynamic Characteristics of Stiffened Rings by Transfer Matrix Approach. Journal of Sound and Vibration 39, 237-245 (1975).

18. V. R. Murthy and T. J. McDaniel, Solution Bounds to Structural Systems. AIAA Journal 14, 111-113 (1976).

19. T. J. McDaniel and V. R. Murthy, Solution Bounds for Varying Geometry Beams. Journal of Sound and Vibration 44, 431-448 (1976).

20. W. P. Targoff, The Bending Vibrations of a Twisted Rotating Beam. Proceedings of the Third Midwestern Conference on Solid Mechanics, 177-197 (1957).

21. G. Isakson and G. J. Eisley, Natural Frequencies in Bending of Twisted Rotating Blades. NASA TN D-371 (1960).

22. G. Isakson and G. J. Eisley, Natural Frequencies in Coupled Bending and Torsion of Twisted Rotating and Non-Rotating Blades. NASA CR-65 (1964).

23. V. R. Murthy, Dynamic Characteristics of Rotor Blades. Journal of Sound and Vibration 4559, 483-500 (1976).

24. V. R. Murthy and G. A. Pierce, Effect of Phase Angle on Multi-Blade Rotor Flutter. Journal of Sound and Vibration 48, 221-234 (1976).

25. T. J. McDaniel and V. R. Murthy, Bounds on the Dynamic Characteristics of Rotating Beams. AIAA Journal 15, 439-442 (1977).

26. V. R. Murthy and C. E. Hammond, Vibration Analysis of Rotor Blades with Pendulum Absorbers. Journal of Aircraft 18, 23-29 (1981).

27. T. McLarty et al, Rotorcraft Flight Simulation with Coupled Rotor Aeroelastic Stability Analysis. USA AMRDL TR-76-41A (1977).

28. E. R. Wood et al, Implementation and Veritification of a Comprehensive Helicopter Coupled Rotor-Fuselage Analysis. Proceedings of the Theoretical Basis of Helicopter Technology, Nanjing Aeronautical Institute, Nanjing, China (1985).

29. R.L. Bielawa, Aeroelastic Analysis for Helicopter Rotor Blades with Time Variable, Nonlinear Structural Twist and Multiple Structural Redundancy--Mathematical Derivation and Program User's Manual. NASA CR-2638 (1976).

30. W. G. Bousman, R. A. Ormiston, and P. H. Mirick, Design Considerations for Bearingless Main Rotor Hubs. Proceedings of the American Helicopter Society 39th Annual National Forum, 509-536 (1983).

31. P. G. C. Dixon and H. E. Bishop, The Bearingless Main Rotor. Journal of the American Helicopter Society 25, 15-21 (1980).

32. J. L. Sorensen, L. J. Silverthorn and T. H. Maier, Dynamic Characteristics of Advanced Bearingless Rotors at McDonnell Douglas Helicopter Company. Proceedings of the American Helicopter Society 44th Annual Forum, 559-570 (1988).

33. N. T. Sivaneri oand I. Chopra, Finite Element Analysis for Bearingless Rotor Blade Aeroelasticity. Journal of the American Helicopter Society 29, PP 42-51 (1984).

34. V. R. Murthy and A. M. Joshi, Free-Vibration Characteristics of Multiple-Load-Path Blades by the Transfer Matrix Method. Journal of the American Helicopter Society 31, 43-50 (1986).

35. K. B. Sangha, Bearingless Rotors and Higher Harmonic Control Modeling Using RACAP. Proceedings of the American Helicopter Society 44th Annual Forum, 293-304 (1988).

36. D. H. Hodges and E. H. Dowell, Nonlinear Equations of Motion for Elastic Bending and Torsion of Twisted Nonuniform Blades. NASA TN D-7818 (1974).

37. T. Theodorsen, General Theory of Aerodynamic Instability and the Mechanism of Flutter, NACA Report 496, 1935.

38. L. A. Shultz and V. R. Murthy, Direct Application of the Transfer Matrix Method to Solve Nonlinear Autonomous Boundary Value Problems with Multiple Branches. Computers and Structures, 49, No. 3, 439-452 (1993).

39. R. L. Bisplinghoff, H. Ashley and R. L. Halfman, Aeroelasticity. Addison-Wesley Publishing Co. Inc., Reading, Massachusetts (1955).

40. D. H. Hodges and R. A. Ormiston, Stability of Elastic Bending and Torsion of Uniform Cantilever Rotor Blades in Hover with Variable Structural Coupling. NASA TN D-[9102 (1976).

41. A. Gessow and G. C. Myers, Jr., Aerodynamics of the Helicopters. Frederick Ungar Publishing Co., New York (1952).

42. R. E. Bellman and R. E. Kalaba, Quasilinearization and Nonlinear Boundary-Value Problems. American Elsevier Publishing Company, Inc., New York (1965).

43. D. E. Muller, A. Method for Solving Algebraic Equations Using an Automatic Computer, Mathematical Tables and Aids to Computation, No. 10, pp. 208-21, 1955.

44. W. B. Stephens, D. H. Hodges, J. H. Avila and R. M. Kung, Stability of Nonuniform Rotor Blades in Hover Using a Mixed Formulation. Vertica 6, 97-109 (1982).

45. L. A. Shultz, B. Panda, F. J. Tarzanin, R. C. Derham, B., K. Oh, L., Dadone, Interdisciplinary Analysis for Advanced Rotors - Approach, Capabilities and Status, pp. PS4.1 - PS4.15. Proceedings of the American Helicopter Society Aeromechanics Specialists Conference, San Francisco, California, January 1994.

Appendix A: Helpful Integrals to Evaluate the Coefficients Defined in Equations (3.47), (2.48)

$$\int_{1}^{-1} \sqrt{\frac{1-\xi^*}{1+\xi^*}}\, d\xi^* = -\pi$$

$$\int_{1}^{-1} \frac{1-\xi^*}{1+\xi^*}\, \xi^*\, d\xi^* = \text{illegible}$$

$$\int_{1}^{-1} \frac{1-\xi^*}{1+\xi^*}\, \xi^{*2} = -\pi$$

Appendix B: Natural Frequencies of a Nonrotating Uniform Cantilevered Beam

$$\omega_n = (\beta l)_n^2 \sqrt{\frac{EI}{ml^4}} \qquad \text{(Flap, Lag)}$$

where

n	$(\beta l)_n$
1	1.875
2	4.694
3	7.855
>3	$\frac{2n-1}{2}\pi$ (approx)

and

$$\omega_n = \frac{2n-1}{2}\frac{\pi}{l}\sqrt{\frac{GJ}{I}} \qquad \text{(Torsion)}$$

where n = 1,2,3, ...